OPTIMISATION OF OXY-ACETYLENE FLAME SPRAYING PROCESS FOR A Ni BASED COATING USING BOX-BEHNKEN MODEL

by

SAUMYA MUKHERJEE

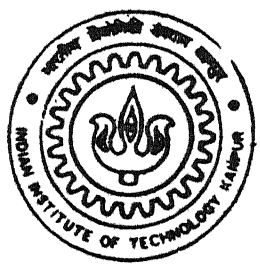

DEPARTMENT OF MATERIALS AND METALLURGICAL ENGINEERING

INDIAN INSTITUTE OF TECHNOLOGY KANPUR

February, 2000

OPTIMISATION OF OXY-ACETYLENE FLAME SPRAYING PROCESS FOR A Ni BASED COATING USING BOX-BEHNKEN MODEL

A Thesis Submitted

in Partial Fulfillment of the Requirements for the Degree of

Master of Technology

by

SAUMYA MUKHERJEE

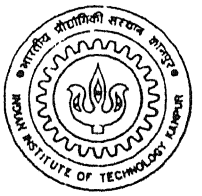

to the

DEPARTMENT OF MATERIALS AND METALLURGICAL ENGINEERING
INDIAN INSTITUTE OF TECHNOLOGY KANPUR

FEBRUARY 2000

CERTIFICATE

It is certified that the work contained in this thesis entitled "*Optimisation of Oxy-Acetylene Flame Spraying Process for a Ni Based Coating Using Box-Behnken Model* ", by Saumya Mukherjee, has been carried out under my supervision and that this work has not been submitted elsewhere for any degree.

Monica Katiyar.

Dr. MONICA KATIYAR
Asst. Professor
Materials and Metallurgical Engineering,
Indian Institute of Technology, Kanpur
February, 2000

Dedicated to .....

My Parents

Acknowledgement

I thank my guide, Dr. Monica Katiyar, for her guidance, inspiration and encouragement during the course of this project. She has taught me the values of research and independent thinking. She spent tremendous time and effort on me and was always ready to help and discuss my difficulties. It was a great pleasure working with her.

I must take the opportunity to thank my friends Badirujjaman, Rohitaswa, Ritwik, Pinaki, Indranil, Mukut , Ajay, Kapil, Shoumitra, Ashish, Sridhar, Somnath and many others for their kind help in completing this thesis. I also would like to thank all the laboratory staffs, Mr. Soni, Mr. Umashankar , Mr.R. P. Singh, Mr. Sharma, Mr. Agnihotri and many others who have helped me a lot, without which this thesis could not have been a reality.

A lot of thanks goes to many of the technicians in 4 BRD Chakeri, Kanpur who have helped me a lot during my early days of experimental works. They helped me heart out all the time I need help from them.

Finally I would mention the contribution of my family members who supplied me constant inspiration throughout my project work. In many times of disgrace and despair they really supplied me the required boost without which I could not even thought of doing this. They do not want their names to be mentioned separately, and their names need not be mentioned also.

Abstract

Thermal spraying techniques have wide range of applications, for example in preparing mining tools, cutting tools, aerospace applications, navy applications, orthopaedic applications, automotive applications and many other and it is a growing field too. However, the spraying process is controlled by its processing parameters in a complex manner and it is very difficult to correlate between the structure and properties of the coating. In my study, an attempt is made to characterise and then optimise the 20B rod spraying process. This is a Ni-based abradable coating used in aeroengines. The Box-Behnken model is chosen to design the experiment using feed rate, stand-off distance (S.O.D.), and compressed air pressure (C.A.P.) as the processing parameters. Hardness of the coating and the volume fraction of the powder phase are taken as the response variables. After the statistical analysis of the data, it is observed that feed rate and S.O.D. have large effect on hardness of the coating while C.A.P. has little effect. Among the interaction effects, both C.A.P. * feed rate and feed rate * S.O.D. are significant while C.A.P. * S.O.D. is nominal. On the other hand, when volume fraction of the powder phase is used as the response variable, effect of feed rate and C.A.P. are found to be large and S.O.D. has a nominal effect. Among the interaction effects, only feed rate * S.O.D. has a significant effect while C.A.P. * feed rate and S.O.D. * C.A.P. have little effects. The process is then optimised with respect to its processing parameters, and it is found that a low value of feed rate and S.O.D. coupled with a high level of C.A.P. can produce a coating with required hardness value and porosity level. This is not surprising since this combination of parameters will result in high temperature and kinetic energy of

the particles hitting the substrate. Feed rate and C.A.P. should be closely controlled in order to limit the hardness value within the specified range.

Deposition of coating using 20B powder was not possible because as-purchased powder is not flowable and cannot be deposited using a 6P-II hand held thermospray gun. So, the dependence of the flowability on the size distribution and shape of the particles is analysed. After the analysis, it is suggested that by narrowing the size distribution of the 20B powder one can spray the coating.

Contents

List of Figures

List of Tables

Chapter 1

Introduction

Thermal spray technology is a rapidly evolving field which interacts with a broad industrial community and has a wide range of important practical applications - for example , mining tools [1], automotive applications [2], navy applications [3], orthopaedic applications [4], cutting tools [5] etc. In general terms thermal spraying involves the deposition, on to a substrate, of a relatively thick solid coating from a stream of molten or partially molten droplets. The droplets normally impact on the substrate at speeds in excess of 150 ms^{-1} depending on the spray process employed. The droplets then spread out to form splats, and rapidly solidify. The coating develops through the formation of successive layers of splats which bond together. Deposited microstructures are extremely complex and are frequently far from equilibrium because of the high cooling rates involved.

Many thermal spraying processes are in use in industries, for example, high velocity oxy-fuel technique, combustion flame spraying, plasma spraying process, wire arc spraying process etc. The microstructures and properties of coatings depend in a complex manner on the processing method and the numerous processing variables of a given method [6]. Several reviews and studies have been published on the microstructural appearance of spray coatings as a function of spraying method [7]. Although a sufficient amount of information is available for most engineering applications of these materials, still it is not possible to

predict structure/property relationship based on the method of deposition. In other words, fundamental relationships between the processing variables, coating structure, and coating properties for different methods need to be studied [8].

1.1 Problem Statement

The technicians of 4BRD Air Force Base, Chakeri use to maintain and repair a lot of aeroengines coming from Indian Air Force. They use a lot of thermal spraying processes in order to repair the damages of the engines. In one of the processes, they deposit a Ni-based coating on to a steel casing using 20B rod (consisting of Ni, Cu, C, BN) oxy-acetylene flame spraying process. This coating is abradable in nature, and they deposit this coating in order to minimise the clearance between the blades and and the outer casing of the engine. The 20B rod is prepared from 20B powder then only it is sprayed. However, the Air Force people find this process costly as the 20B powder needs to be converted into 20B rod and this conversion process is costly. In addition to that, the parameter regimes associated with the 20B rod flame spray process are also very narrow. So considering all these problems, they questioned whether the 20B powder can be directly sprayed using oxy-acetylene flame spray process or not.

As stated earlier, the relationship between the coating properties and the parameters of the process is extremely difficult to find out. So, I decided to approach the problem following the steps listed below.

I) Complete characterisation of the existing 20B rod flame spray process.

II) Effort to deposit 20B powder directly on to the substrate.

III) Characterisation of 20B powder flame spray process and comparison between these two processes.

1.2 Proposed Work

To investigate the first step mentioned above, I first sorted out the most important parameters associated with the 20B rod flame spraying process. The feed rate, the stand-off distance, and the compressed air pressure are chosen to be the three most important parameters as the oxygen/acetylene ratio cannot be changed. Then for correlation analysis a statistical factorial plan was used to assess the effects of the parameters. Detail microstructural studies were carried out using optical microscopy and SEM to find out the coating structure. To find out how the different elements are distributed throughout the structure EPMA was carried out. XRD was done on the 20B rod and the coating to find out the constituents. As a representative of the mechanical properties hardness testing was done.

The 20B powder was found to be non-sprayable as the powder was not flowing. So, I decided to characterise the powder properties. In doing that, I first screened the powder into different size fractions and then measured the flowability of different size fractions. Then to check the chemical homogeneity of the powder, quantitative analysis of different constituent was done on certain size fraction of the 20B powder using XRD analysis. SEM photographs of the 20B powder was also taken to check the shape of the powder.

After the investigations the optimum parameter regimes of the 20B rod coating process are suggested. Different parameter interactions and the cross effects are also reported. Complete characterisation of the 20B powder is done as it cannot be sprayed directly, and possible ways of powder deposition using flame spraying technique are suggested.

1.3 Organisation of Thesis

Rest of the thesis is divided in five more chapters. In the second chapter I have reviewed many pertinent literatures which deal with many important features in the field of thermal spraying technology. In the third chapter I have given the entire methodology following

which I have conducted my experiments. In the fourth chapter I have given all the results, tables , and figures obtained from different experiments I have conducted and then I have discussed my results. In the fifth chapter I have drawn the conclusions. In the last chapter I have suggested some relevant future works.

Chapter 2

Literature Review

Thermal spray coatings have become an important part of modern industry, offering customised surface properties for a variety of industrial applications ranging from thermal barrier coatings for high tech turbine blades to erosion resistant coatings for boiler tubes. Thermal spraying is the generic name for a family of thick overlay processes in which a material is heated rapidly to near its melting point in hot gaseous medium and then projected at high velocity on to a prepared substrate surface to build up the desired coating [9]. The substrate should be sufficiently massive so that it can absorb heat from the molten coating material to let them solidify and at the same time can protect itself from becoming too hot . The droplets then impact on the substrate and adhere to it most probably by mechanical interlocking which is nothing but a physical keying between an often deliberately roughened substrate and a coating that is in close contact with the substrate [10]. Nowadays it is possible to spray virtually all the materials provided these melt or become substantially molten without being degraded significantly during a short residence in the heat source. Despite its inherent complexity thermal spraying is an established route for the protection of conventional engineering materials to allow them to function under extreme conditions of aggressive wear, corrosion, or high temperature. Furthermore, the application of thermal sprayed protective layers has often been the key to enabling novel, high performance base

materials to find practical applications [6].

In this chapter, at first I would give an overview of the major thermal spray processes in operation, and then I would discuss the characterisation procedure of the sprayed coatings, bonding mechanism of thermal sprayed coatings, the basic principles of flame spraying process gradually in subsequent sections. Then at last I would briefly discuss the major process parameters of flame spraying as my thesis deals with this combustion flame spraying process.

2.1 Thermal Spraying Processes

A variety of thermal spraying processes are available for the deposition of coatings. The principal techniques are combustion flame spraying, arc wire spraying, high velocity combustion and plasma spraying. The basic charac teristics of the processes are briefly described here.

2.1.1 Combustion Flame Spraying

In this process an oxygen/acetylene mixture is passed through a nozzle and ignited to form a combustion flame, accelerated and projected onto the substrate surface to form the coating deposit (Figure 2.1). The combustion flame temperature is limited to some 3000°C temperature and gas/particle velocities are relatively slow. Thus the types of coating material to be deposited are restricted and the deposit itself tends to be porous, poorly bonded and in the case of metallic coatings exhibits a high oxide content. Flame spraying is the cheapest of the thermal spraying processes and can be used successfully for some applications, mainly where porosity or high oxide levels provide specific benefits. For example, oil retention for bearings and hard molybdenum coatings for piston rings can be mentioned. The technique can also be used to deposit self fluxing systems (systems in which the coating constituents react among each other to form a product which protect the coating from atmospheric attack) such as Ni-Cr-B-Si which can be fused to form wear resistant layers.

2.1.2 Arc Wire Spraying

This process involves the production of molten particles at the tips of two consumable wires via resistance heating (Figure 2.2). The material is subsequently atomised and projected onto the substrate by a compressed air jet. The process is limited to spraying of conductive wires, the spray material is initially fully molten and reaches higher velocities in this process than in flame spraying. The coatings deposited by this process are more dense and highly bonded than flame spray systems. The arc wire process is relatively cheap and can achieve high deposition rates.

2.1.3 High Velocity Combustion Processes

There are two principal high velocity combustion processes: Detonation Gun and Jet-Kote. Both processes generate high powder velocities and deposit coatings of higher density and bond strengths than flame and arc wire techniques.

The Detonation Gun

The Detonation Gun or D-Gun is a process developed by Union Carbide which utilises the energy released by a controlled series of detonations of oxygen and acetylene to heat and accelerate the coating powder to high velocities and propel them onto prepared surfaces to form coatings. Measured volumes of oxygen and acetylene are fed into a combustion chamber at the breech of a gun barrel as shown in Figure 2.3. Fine coating powder is introduced via a separate port. The gas mixture is ignited by an electric spark. A detonation occurs causing a temperature increase to around 4000°C. The high temperature gases leaving the gun along the barrel cause the particles to be accelerated, plastically deformed and ejected from the gun at 750 ms^{-1}. On impact on the target, their high kinetic energy produces a strong bond with the substrate or the previously coated layer. After detonation the D-Gun is purged with nitrogen and the process is repeated (4-8) times per second to build up the coating

to the required thickness. Gas temperatures associated with the D-Gun are some 1000°C hotter than with conventional oxy- acetylene torches but components to be coated are cooled during processing by supplimentary cooling. The resulting coatings are of high density, high quality and relatively free of inclusions and unprocessed particles.

Jet-Kote

This process is based upon rocket motor design and produces a high velocity combustion gas jet (Figure 2.4). As with D-Gun, the process deposits high density well-bonded coatings. The basic differences with these high velocity combustion processes and the ordinary combustion process lie in the fact that in the former processes the reaction between oxygen and fuel occur under inequilibrium condition which create that extra temperature while the free burning temperature of oxygen and fuel is relatively low.

2.1.4 Plasma Spraying Processes

The plasma gun comprises a copper anode and tungsten cathode, both of which are water-cooled. An inert gas, usually argon, flows around the cathode and through the anode which is shaped as a constricted nozzle. Gases other than argon,such as nitrogen, helium or hydrogen (used as a secondary gas) can also be used. A DC arc is initiated between the electrodes by a high voltage discharge, ionising the gas, with the resulting plasma exiting the gun via the nozzle, thereby producing a high velocity jet. The coating material in fine powder form is injected into the plasma, resulting in plastic particles (molten or semi-molten) which are accelerated and propelled onto prepared surfaces so that they deform and adhere on impact to form a coating. Plasma spraying is performed using three principal techniques: air plasma spraying(APS) (Figure 2.5), argon-shrouded plasma spraying(ASPS) and vacuum plasma spraying (VPS) (Figure 2.6).

In air plasma spraying the powder particles are rendered plastically deformable and accelerated to (200-400)ms^{-1} before being deposited as relatively dense coatings. The main

imitation of this technique is the incorporation of air in the plasma jet, thereby cooling and slowing the plasma and causing some oxidation of metallic or alloy powder, consequently depositing coatings with significant contamination. However, when oxide contamination in coatings is tolerable, for example in the case of air sprayed M-Cr-Al-X (where M stands for metals like Fe and Ni, and X stands for metals like Y) bond coats in the thermal barrier coatings systems the APS provides satisfactory result. It is also observed in the case of thermal barrier coating made of ZrO_2-Y_2O_3 layer which is often used in combustion chambers of gas turbine engines. coatings.

In argon shrouded plasma spraying, the use of an argon gas shield around the plasma gun and workpiece provides protection against the deleterious of air encountered with the APS technique. Consequently,the ASPS coatings are clean, well-bonded and relatively oxide-free compared with APS deposits. Typical applications of ASPS include M-Cr-Al-X systems for turbine hot section components.

The vacuum plasma spraying process, sometimes termed low pressure plasma spraying, has several advantages over air spraying. The advantage of VPS is that it can achieve (400-600) ms^{-1} particle velocities with the overall result being the deposition of highly dense high purity deposits. A further significant advantage of VPS is coating adhesion. In vacuum a transferred arc can be utilised to sputter clean the substrate surface prior to the coating process, consequently giving a clean coating-substrate interface and promoting adhesion. The use of a vacuum chamber also permits the heating of the component to high temperatures to promote diffusional bonding without oxidation problems. Typical VPS applications in aero engines include M-Cr-Al-X systems as overlay coatings or TBC (thermal barrier coatings) bond coats for the protection of hot section components [11].

2.2 Characterisation Procedure of Thermal Sprayed Coatings

Although the usage of thermal sprayed coatings has increased dramatically, the characterisation and analysis of these coatings has lagged behind. Characterisation is critical for understanding why thermal spray coatings behave the way they do, and offering guidelines for improved coating performance in the future.

Thermal spray coatings are formed by melting materials in particulate form or wire feed stock and accelerating the molten droplets toward a substrate. Once these molten droplets strike the substrate they expand out in a radial fashion and form a splat. As additional particles impact the specimen, splats will eventually interact with one another and form a continuous coating. Splat-to-substrate, as well as splat-to-splat, bonding tends to be weak, providing little resistance to pullout during the mechanical processing (cutti ng , grinding, and polishing) of the coating for metallographic preparation. In addition, multiphase coatings, such as cermets, can have enhanced pullout due to the differant sizes and densities of the as-sprayed powders. Consequently, if care is not taken when preparing a thermal spray coating for analysis, pullout can cause erroneous porosity, volume percent, and even chemistry measurements.

Although there has been some work on metallographic preparation and routine examination of thermal spray materials, few studies have done thorough examinations of both chemistry and physical structure of the as-sprayed coating. In this section, an attempt is made to explore some basic sample preparation methodologies and in depth techniques for analysis of complex as sprayed coatings is provided. The analysis of coatings centers on quantifyi ng the structure of the coating and determining the chemical makeup of the variou s phases in the coating. The experimental procedure is illustrated here using a specific example of FeCrAlY-Cr_2C_3 cermet coating [14]. First, the carbide ranges sprayed and the chemical composition of the pre-sprayed powders are reported in Table 2.2 and Table 2.3.

FeCrAlY-Cr_3C_2 cermet coatings are applied to low carbon steel substrates using a HVOF spray system. Next, chemical, structural, and mechanical properties are measured.

2.2.1 Structural Characterisation

Once the samples were sprayed, the coatings were sectioned on a low speed abrasive cut off saw and vacuum mounted in epoxy mixed with a fluorescent dye. The configuration of the mounted samples is shown in Figure 2.7. The samples were mounted coating-to-coating to help maintain the coatings edge and avoid rounding. The samples were then ground through 600 grit using SiC papers, polished to 1 μm diamond with a low nap cloth on a polisher, and finally polished with colloidal silica for 15 minutes on a vibratory polisher. Finally, the coatings were etched with various chemicals as required. The coatings were first photographed using light optical microscopy (LOM) in addition to a JEOL scanning electron microscopy to provide preliminary phase identification. The Reikert LOM was used in Nomarski mode to enhance the contrast of the HVOF coatings and allow detailed analysis of the coating inter-splat structure. X-ray diffraction patterns of all of the coatings were obtained using a Siemens diffractometer. In this case, the coatings were removed from their substrates and broken up using liquid nitrogen prior to testing. WDS (wave dispersive X-ray) dot maps were also used to help with phase determination and confirm the x-ray data using a JEOL superprobe.

2.2.2 Chemical Characterisation

The chemistry of the individual phases that comprised each coating were determined using several complementary methods such as XRD and WDS. Once the chemical nature of each phase had been determined the coatings were then quantified using a LECO 2001 image analysis system. The volume percent of each phase, in addition to the thickness of each coating, was determined. Since the carbide and FeCrAlY matrix had similar gray levels

the matrix had to be etched away using a HCl-HNO_3 etch. With FeCrAlY matrix gone all of of the phases could be easily be distinguished by thresholding [15]. Other chemical characterisations like the corrosion resistance of the coating can also be done.

2.2.3 Mechanical Characterisation

Finally, microhardness measurements of each phase were also conducted to complete the qualitative chemical analysis of the various coatings. In general, many other testings can also be done to reveal some important properties of coating. These include wear testing to judge the abrasion resistance of the coating, adhesion testing to measure the bond strength of the coating and many other.

2.3 Bonding Mechanism of Thermally Sprayed Coatings

Along with the increasing number of applications for sprayed coatings, there has been a demand for coatings of higher quality. One of the indispensable characteristics of high-quality sprayed coatings is strong adhesion to the substrate. Accordingly, a fundamental consideration for insuring coating adhesion is an understanding of the adhesive mechanism and the composition of the boundary between the sprayed coating and the substrate. Because the coating is formed by depositing high-velocity finely sprayed particles onto the substrate surface, the boundary between the coating and the substrate has an exceedingly fine structure, and a revealing experiment on it is very difficult. Therefore, it is not surprising that one finds few reports on the adhesive mechanism and the composition of the boundary. Next, I will discuss the adhesive mechanism of the nickel, chromium, molybdenum, tantalum and tungsten coatings deposited by a plasma jet spraying on to aluminium and mild steel substrates [14]. This study was done by the examination of oblique metallographic sections and by electron beam probe measurement (EPMA) of the concentration distribution of elements

at the boundary between the coating and the substrate. The composition of the boundary layer was also analyzed by X-ray diffraction. The relationship between the tensile strength and the structure of the boundary was also determined. In addition, in order to confirm the nature of the adhesive mechanism and its dependence on the composition of the boundary layer, an analog experiment using the levitation melting process was carried out. Spraying materials used in this experiment were Mo, Ta and W which have high melting points, and Ni and Cr which have intermediate melting points. Each was in powder form of mesh size ranging from -200 to +325. Aluminium and mild steel substrates were used for spraying. A Plasmatron PM-322 plasma jet generator and a SG-1B type torch was used, and spraying was done in air. The operating conditions are listed below in Table 2.4.

To clarify the adhesive mechanism at the boundary between the coating and the substrate, an analysis of the elements in the boundary layer was made for each specimen using an EPMA. On an oblique section of each specimen, a linear scan along the direction perpendicular to the boundary face was made in order to determine the concentration distribution of the elements in the coating and substrate boundary layer.

One end face of Al and mild steel bars which had been polished chemically was preheated to 100°C by means of a plasma jet flame, and then coated with each material to a thickness of about 0.3mm. Tensile testing was carried out and the tensile strength was determined by dividing the maximum rupture load by the cross-sectional area of the bar. The tensile test results are shown in Table 2.5.

CuK_α and CoK_α radiations which are used for X-ray diffraction analysis have a high penetrating power in these metals. Therefore, the composition of the adhesive layer formed at the boundary between the coating and the substrate can be analysed from the substrate side using X-rays, if a foil substrate is used. In this case, the thickness of the substrate must be smaller than the depth of the X-ray penetration. Therefore, the effective depth of X-ray penetration in aluminium and mild steel was investigated in order to choose a proper

thickness for the substrates. The effective depth of X-ray penetration can be calculated from the following formulas.

$$X = K_x \sin\theta/2\mu \tag{2.1}$$

$$K_x = \ln(1/1 - G_x) \tag{2.2}$$

$$\tag{2.3}$$

where X is the effective depth of X-ray penetration, μ is the linear absorption coefficient, θ is the angle between the incident X-ray and the specimen surface, G_x is the ratio of the total integrated intensity diffracted by a specimen of thickness X to that diffracted by a specimen of infinite thickness.

The results of this calculation are shown in Table 2.6 while Table 2.7 gives the components of the interfacial layer using X-ray analysis. The results of the experiments are summarised as follows:

1. The formations of boundary layers between the plasma jet sprayed coating and the substrate was confirmed through observation of the boundary using an optical microscope. The layers were formed partially when Ni or Cr was sprayed onto a mild steel substrate, and were formed all along the boundary length in the other cases.

2. From the measurement of the concentration distribution of elements in the boundary layer by means of an electron probe X-ray microanalyser, it is clear that the boundary layer between the coating and the substrate is formed metallurgically.

3. From the results of the tensile test, for those coating and substrate combinations which adhere metallurgically and form a boundary layer, the adhesive strength was higher than the cohesive strength of the coating itself. In the Ni and Cr coating which adhered mainly by mechanical bonding onto mild steel substrate, rupture occurred at the boundary between the coating and the substrate. Thus, it is clear that a boundary layer formed between the coating and the substrate is necessary to improve the adhesion of a sprayed

4. It was confirmed by X-ray diffraction analysis that the boundary layer between the sprayed coating and a foil substrate consists of intermetallic compounds of the elements of the coating and substrate materials. From these results, it was also demonstrated that the substrate surface was melted the moment the sprayed particles impinged on the substrate.

5. The adhesive mechanism of coatings sprayed onto substrate surfaces and the composition of the boundary layer were further demonstrated by carrying out an analog experiment using the levitation melting process [14]. This levitation melting process involves preparation of a molten nickel drop and allowing it to drop on to Al and mild steel substrates. This prolong the reaction time between the sprayed particles and substrate, and in the process increase the quantity of the substances produced at the boundary.

2.4 The Basic Principle of Flame Spraying

In broad sense, flame spraying processes are divided in two categories - one utilising material to be deposited in wire form and designated "wire combustion spray", and the second utilising material in powder form and designated as "Powder Combustion Spray" [16]. Both processes use a combustion flame as a heat source.

2.4.1 The Wire Combustion Spray Process

Figure 2.8 shows how this process can be subdivided into the following:

A. The Process Occurring at the Source

As illustrated in the figure, the source comprises a nozzle, through the centre of which wire is passed into an oxy-fuel flame. An annulus is formed around the outside of the nozzle, and the inside of an air cap, through which compressed air is fed. The wire tip is continuously heated to its melting point, and then broken down into particles by the stream of compressed

air.

B. The Process Occurring in Transport

Molten particles are accelerated by virtue of the air stream towards the substrate. In doing so, they are both cooled to a plastic or a semi-molten condition, and a certain amount of oxidation occurs on the particle surfaces.

C. The Process Occurring on Impact with the Substrate

Upon impact with the substrate the particles flatten and bond to it. Subsequent particles also flatten, and bond to those already adhered to the substrate, thereby fabricating a coating.

2.4.2 The Powder Combustion Spray Process

Figure 2.9 illustrates how this process can be readily subdivided into the following:

A. The Process Occurring at the Source

The source essentially comprises of a nozzle, through the centre of which material in powder form can be conveyed by being suspended in a carrier or aspirating gas. The material passes out of the nozzle into an oxy-fuel flame, and is thereby raised to a temperature approaching its melting point.

B. The Process Occurring in Transport

The flame velocity accelerates the semi-molten particles towards the substrate. In so doing there will be a certain amount of oxidation on the particle surfaces. Compressed air may be used further to accelerate particles, thereby producing higher particle velocities.

The Process Occurring at the Substrate

The process occurring at the substrate is certainly the same as that described in the wire combustion spray process.

2.5 Major Parameters Associated with Flame Spraying Processes

A lot of process parameters control the flame spraying process. By minutely controlling some of these parameters an experienced operator can effectively manipulate the coating quality. In this section some of the most important parameters associated with flame spraying process are briefly discussed, since my thesis is related to flame spraying technique [12, 13].

2.5.1 Stand-Off Distance

Stand-off distance is a significant parameter in almost every thermal spraying processes. It is the distance between the tip of the spraying nozzle to the substrate surface. In case of high velocity oxy-fuel technique, it plays an important role in controlling the oxygen content of the resultant coating. Increasing it from a baseline of 250mm to beyond 300mm reduces the oxygen content by roughly a third. The reason for this is that hot combustion gases increase oxidation by atmospheric oxygen entraining the flame jet and blowing onto the hot surface when close enough. The entrainment of atmospheric oxygen into the spray jet was also confirmed by other research workers like C. M. Hackett and G. S. Settles [12]. By increasing the spray distance, the heat load on the substrate is reduced thus supressing severe oxidation. This can be measured by thermocouples attached to a bore in the back side of the substrate. By increasi ng stand-off distance the temperature drops from 260°C to below 150°C .

In another experiment, reducing the stand-off distance from 225mm to 150mm, whic

h means an increase in the velocity of impact of 30%, further improved the hardness of the surface [13]. Yet another decrease in this distance from the spray gun overheated the substrate material, causing the coating to loosen .

2.5.2 Feed Rate of The Coating Material

An increase of the powder feed rate has a reducing effect on oxide content in case of high velocity oxy-fuel technique. This supposedly can be explained by two reasons. On the one hand, increasing the amount of spray material at consta nt combustion power results in lower specific heat offer for a single spray particle, thus reducing melting and oxidation tendency during flight and flattening. Metallographic investigations showed that coating with the lowest oxygen content mainly consists of unmelted particles which do not show any oxidation. In contrast, particles which have been completely melted clearly sho w oxide phases. On the other hand, a higher powder feed rate requires a fewer number of passes to build up the coating thickness; by which the effect of hot combustion gases on the surface while passing can be lowered. However, it has to be considered that thicker coating layers per pass to build up a desired thickness will result in higher residual stress [12].

2.5.3 Powder Carrier Gas

The amount of powder carrier gas has a negligible influence on oxygen content of the coating. Thus it can be adjusted for optimum powder transport means. Apparently, even high amounts of carrier gas do not significantly cool down flame jet to reduce the degree of particle melting. The effect of compressed air pressure is significant on the coating quality in case of flame spraying systems as its job is to carry the molten particles to the substrate surface. Higher the compressed air pressure higher will be the velocity and momentum of the particles and higher will be the chance of forming denser coating.

h means an increase in the velocity of impact of 30%, further improved the hardness of the surface [13]. Yet another decrease in this distance from the spray gun overheated the substrate material, causing the coating to loosen .

2.5.2 Feed Rate of The Coating Material

An increase of the powder feed rate has a reducing effect on oxide content in case of high velocity oxy-fuel technique. This supposedly can be explained by two reasons. On the one hand, increasing the amount of spray material at consta nt combustion power results in lower specific heat offer for a single spray particle, thus reducing melting and oxidation tendency during flight and flattening. Metallographic investigations showed that coating with the lowest oxygen content mainly consists of unmelted particles which do not show any oxidation. In contrast, particles which have been completely melted clearly sho w oxide phases. On the other hand, a higher powder feed rate requires a fewer number of passes to build up the coating thickness; by which the effect of hot combustion gases on the surface while passing can be lowered. However, it has to be considered that thicker coating layers per pass to build up a desired thickness will result in higher residual stress [12].

2.5.3 Powder Carrier Gas

The amount of powder carrier gas has a negligible influence on oxygen content of the coating. Thus it can be adjusted for optimum powder transport means. Apparently, even high amounts of carrier gas do not significantly cool down flame jet to reduce the degree of particle melting. The effect of compressed air pressure is significant on the coating quality in case of flame spraying systems as its job is to carry the molten particles to the substrate surface. Higher the compressed air pressure higher will be the velocity and momentum of the particles and higher will be the chance of forming denser coating.

2.5.4 Fuel/Oxygen Ratio

In a certain experiment, a high H/O ratio is beneficial for low oxide contents in the coatings. By screwing down oxygen for combustion the flame jet cools down and particles do not melt completely. However, decreasing the flame enthal py by such means also decreases the gas velocity. A compromise has to be found here. The best results have been obtained with a H/O ratio of 1 : 0.23 [12]. In general , it can be said that the free burning temperature of the flame is limited by theory and the maximum value of it can never be achieved as there is certain heat losses in the process. So, keeping an eye to all the factors like the flame temperature, the degree of plasticity of the particles, the chances of oxide contamination, and the particle velocity is extremely difficult and to find out an optimum fuel/oxygen ratio is a challenging aspect.

2.5.5 Substrate Temperature

According to the experiments using single parameter variation, keeping substrate temperature low is beneficial to get low oxide containing coatings. Assuming equal spray conditions, for substrate temperature reaching around 260°C the released coating oxy gen contents goes upto 2.3 wt%, whereas in cooling down the substrate to 150°C (by compressed air), the oxygen level was around 1.1 wt% [12]. This could be explained by lower oxygen reactivity of the coating top when temperatures are lower. Furthermore, substrate temperatures significantly determine flattening mechanis ms of single particles governing such on-substrate oxidation.

2.5.6 Substrate Preparation

Substrate surface preparation is an important parameter as it dictates the adhesion or bonding of the coating to the substrate. The substrate surface is often grit blasted using

sand or other abrasing material. Hence, the grit size and the grit blasting pressures are also important secondary parameters as these dictate the surface preparation of the substrate.

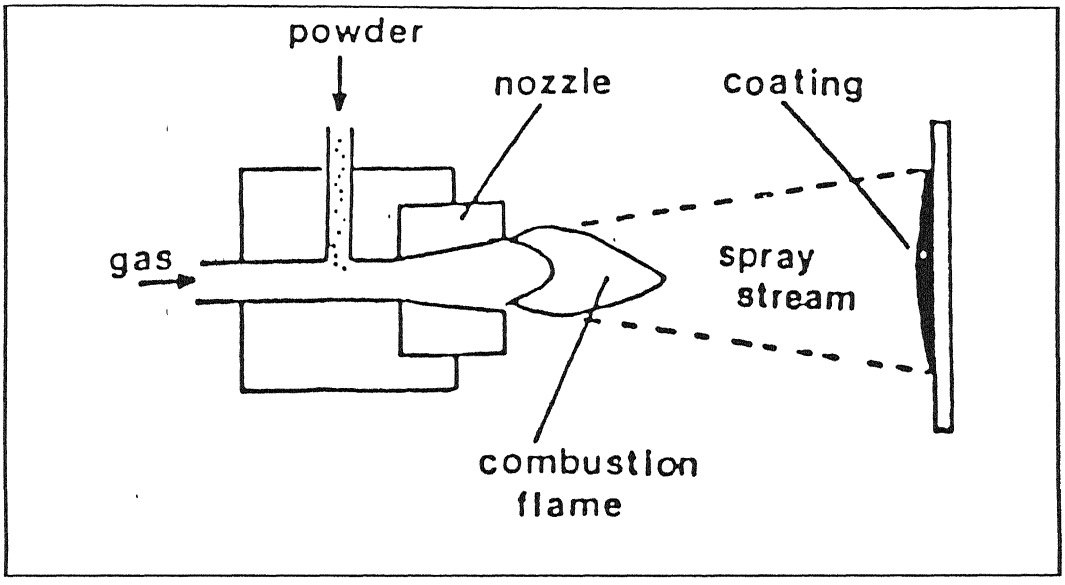

Figure 2.1: Schematic representation of the combustion flame spraying process[11].

Process	Flame	Arc	Plasma	D-Gun
Consumable Material	Powder or Wire	Wire	Powder	Powder
Heat Source	Chemical Reaction	Electric Arc	Inert Gas Plasma	Controlled Ex pl
Flame Temp(^oC)	(2000-4000)	4000	(4500-20000)	3300
Particle Vel(ms^{-1})	(90-180)	240	(240-600)	730

Table 2.1: Principal characteristics of thermal spray deposition processes [11]

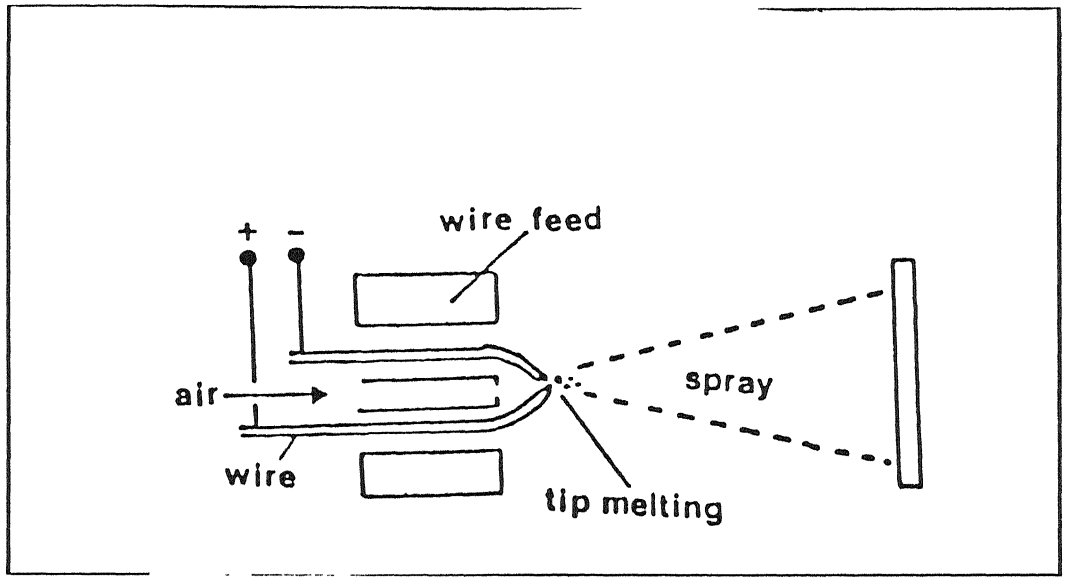

Figure 2.2: Schematic representation of the arc wire spraying process.

Powder Type	Al	C	Cr	Fe	Ni	Y	Other
FeCrAlY	6.5	-	28.50	balance	-	0.65	¡1.00
Cr_3C_2	-	12.75	86.00	-	-	-	¡1.25

Table 2.2: Reported chemistry and compositions of pre-sprayed powders (all values are wt%)

sl.no	weight % FeCrAlY	weight % Cr_3C_2
1	100	0
2	65	35
3	75	25
4	85	15
5	90	10
6	95	5

Table 2.3: Starting powder composition

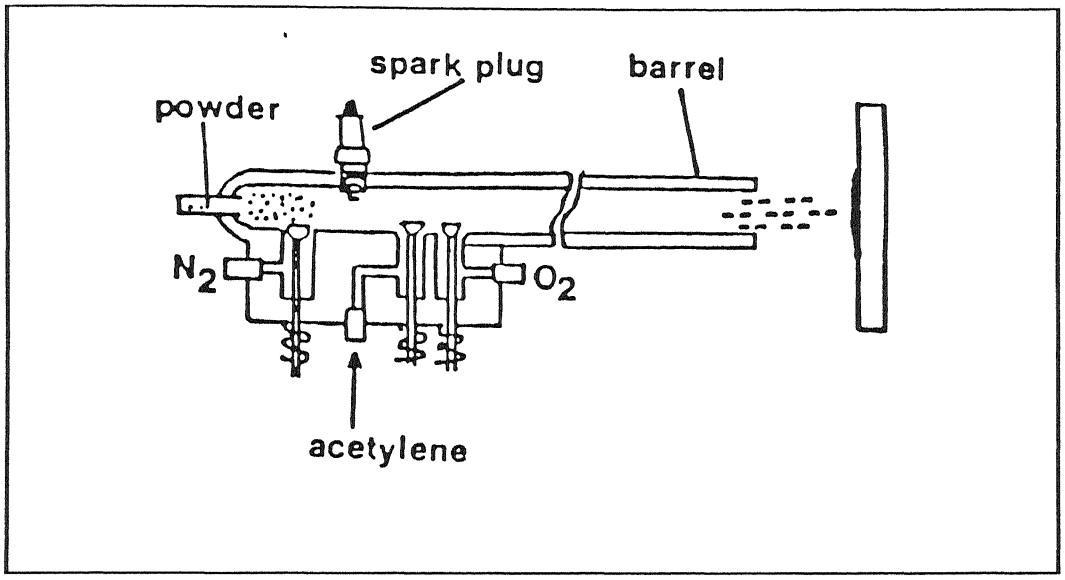

Figure 2.3: Schematic representation of the Detonation Gun spraying process.

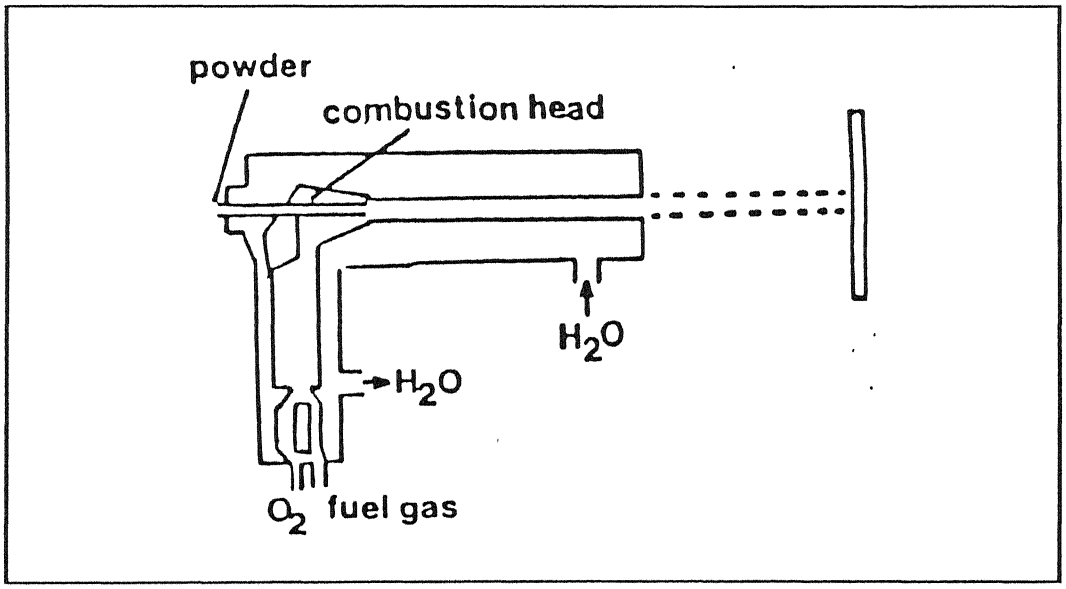

Figure 2.4: Schematic representation of the Jet-Kote spraying process.

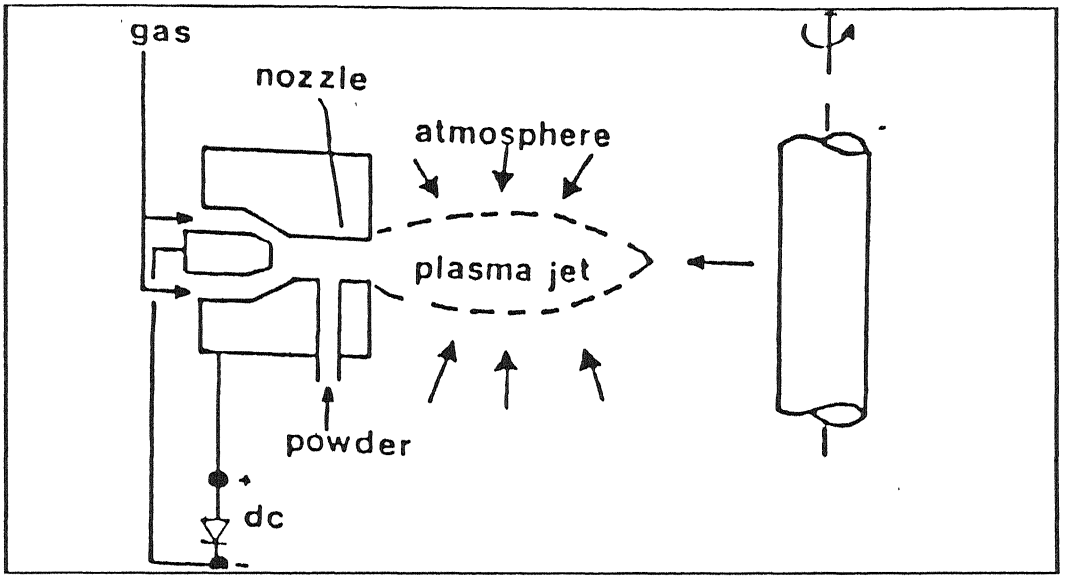

Figure 2.5: Schematic representation of the air plasma spraying process.

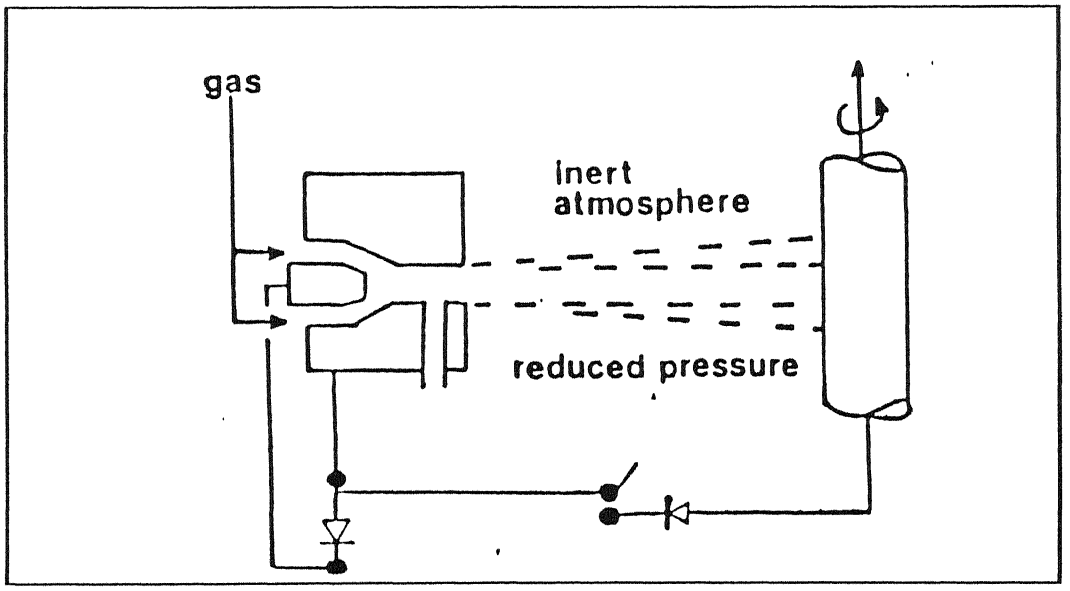

Figure 2.6: Schematic representation of the vacuum plasma spraying process.

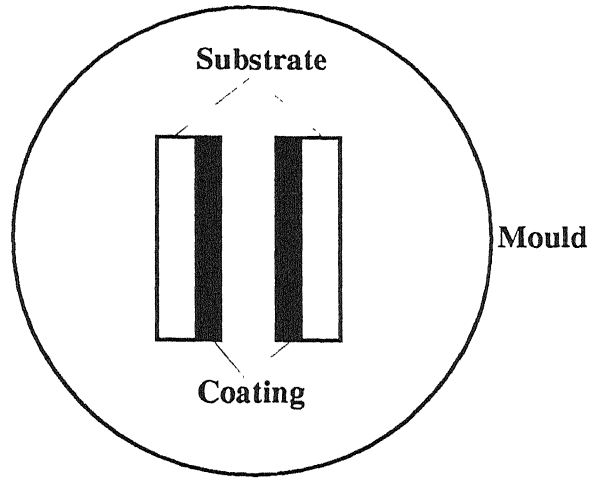

Figure 2.7: Schematic of mounted sample.

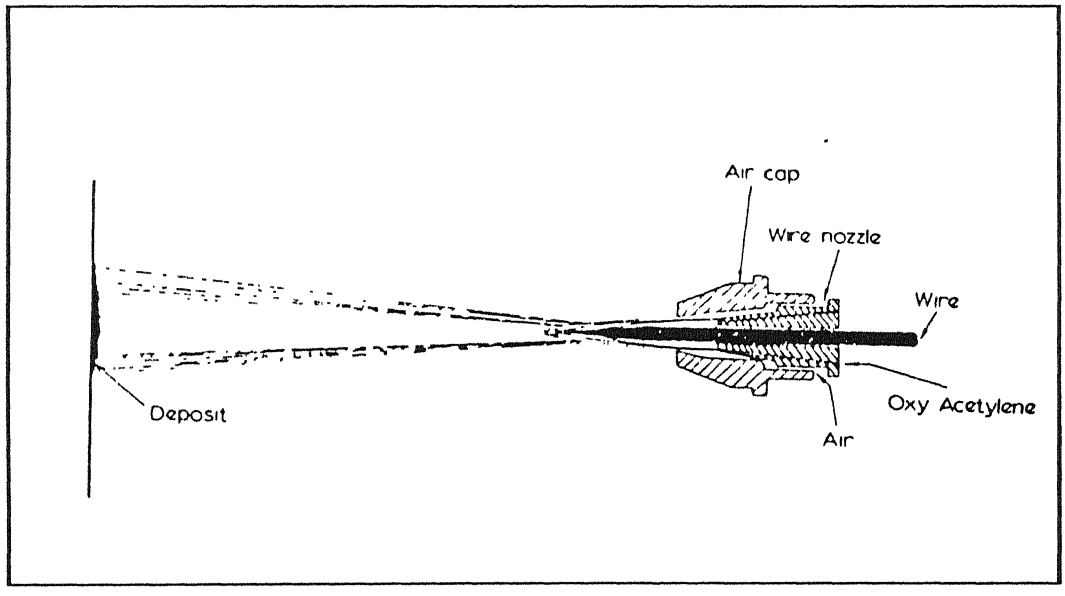

Figure 2.8: Schematic representation of the wire combustion spraying process.

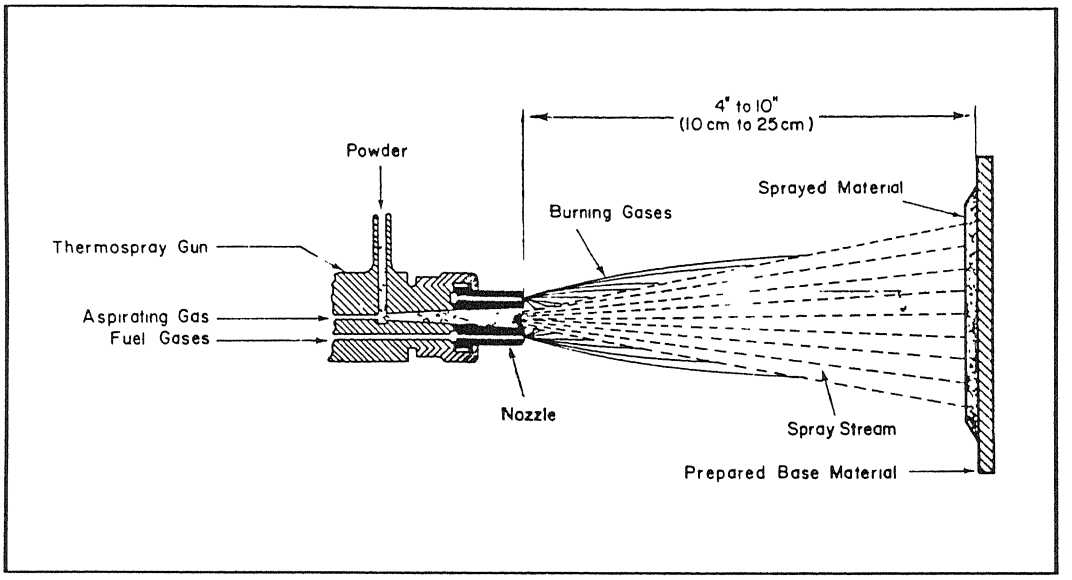

Figure 2.9: Schematic representation of the powder combustion spraying process.

Operating Current	(450-600)Amp
Operating Voltage	(28-32)V
Operating Gas	Ar:30 litre/min
Gas for Powder Supply	Ar:(3-5) litre/min
Spraying Distance	90mm

Table 2.4: Spraying conditions

	Substrate	Al	Mild Steel
Coating		Tensile strength(Kg/mm^2)	Tensile Strength(Kg/mm^2)
Ni		1.4	0.6
Cr		1.4	0.7
Mo		2.3	2.0
Ta		1.3	1.5
W		2.9	2.5

Table 2.5: Results of tensile test

	Diffraction Angle(degree)		2θ	
X-ray		30^o	60^o	90^o
CoKα	Al-substrate	30.1	58.1	81.4
CoKα	Mild Steel-substrate	12.8	24.6	34.5
CuKα	Al-substrate	45.4	87.6	123.0

Table 2.6: The effective depth of X-ray penetration to substrate

Coating	Ni	Cr	Mo	Ta	W
Al-Substrate	Al_3Ni	Al_5Cr	Al_3Mo	Al_2Ta	WAl_{12}
hline Mild Steel-Substrate	....	....	Fe_2Mo	Fe_7Ta_3	Fe_2W

Table 2.7: Compositions of boundary layers between coating and substrate

Chapter 3

Experimental Procedure

In this work the major experimental steps are :

1. The deposition process of 20B rod.

2. Characterisation procedures of the deposited coating.

a) Hardness testing on those coated substrates.

b) Metallographic sample preparation.

c) Light optical microscopy.

d) Scanning electron microscopy.

e) X-ray diffraction pattern identification.

f) Electron probe microanalysis.

3. Characterisation of 20B powder.

Each of these experimental steps is now explained in details below. As in the previous section both the wire feed and the powder feed combustion flame spray processes have been discussed so there is no need of discussing it further. So we can now discuss about the design of experiment keeping a special eye on my own work. In between the discussion, my own experimental steps regarding the 20B rod deposition will automatically come up.

3.1 Design of Experiment

Two response variables in the form of the hardness value of the coating and the volume fraction of the powder phase were taken. These two responses were chosen for some reason. Hardness represents the mechanical property of the coating while the porosity level of the coating is one physical property of the deposited coating. Three parameters were chosen and the effect of these parameters on the two responses were analysed using the Box-Behnken model. The three parameters chosen from the spraying process were feed rate of the 20B rod, jet air pressure, and stand-off distance. The gas ratio, for example, the oxygen/acetylene ratio cannot be varied in the experiment due to some back-firing problem. The other factors like substrate temperature, grit blasting conditions, preheating temperature of 20B rod were kept fixed as much as possible. I chosen a statistical design in which three parameters were varied at three different levels according to Box-Behnken model with single replicate. The Box-Behnken model is shown in Table 3.1 [17].

By -1, 1, 0 in Table 3.1 the three different levels of each parameter are indicated. In our case -1, 1, and 0 depict low, high, and intermediate levels respectively. The three variables, i.e, X_1, X_2, and X_3 indicate feed rate, stand-off distance, and jet air pressure respectively. The exact numerical values of different levels of each parameter are listed in table 3.2. Fixing the numerical values of each parameter at the planned levels and then following the Box-Behnken model fifteen steel samples were sprayed using 20B rod oxy-acetylene flame spraying technique. The 20B rod is composed of nickel, boron nitride, carbon, and copper at specific percentage mentioned in table 3.3. 20B rod is extruded from 20B powder using sodium silicate binder and baked at nearabout 80°C prior to be used in spraying.

A designed experiment is a series of tests in which purposeful changes in the input variables of a process or system lead to the observation and identification of the reasons

for the changes in the output response. We can visualise the process as a combination of machines, methods, people, and other resources that transforms some input into an output that has one or more observable responses. The objectives of the experiment may include the following :

I) Determining which variables are most influential on the response.

II) Determining where to set the influential variables so that the response is almost always near the desired nominal value.

III) Determining where to set the influential variables so that variability in the response is small.

Box and Behnken (1960) have proposed some three level designs for fitting response surfaces. These designs are formed by combining 2^K factorials with incomplete block designs. The resulting designs are usually very efficient in terms of the number of required runs, and they are rotatable (or nearly rotatable). In this context it is worthwhile to mention that an experimental design is said to be rotatable if the variance of the predicted response at some point is a function of the distance of the point from the design centre only and is not a function of direction. A design with this property will leave the variance of the response unchanged when the design is rotated about the centre (0, 0, 0,.....); hence given the name rotatable. The Box-Behnken design does not contain any points at the vertices of the cubic region created by the upper and lower limits of each variable.

I have deposited the coating on the fifteen samples following the statistical model described above. The steel substrates were first cut to required size, i.e, (2 X 40 X 40)mm rectangular pieces using a sheer cutter and then cleaned thoroughly so that no dust, moisture, or grease get chance to stick to it. The substrates were then taken to the grit blasting unit for preparation of surfaces. The abrasive particles used is sand and of -120 mesh size. The grit blasting pressure used in the process is 4 kg/cm^2. After the substrates were grit

strates were grit blasted these were taken to 20B rod fed oxy-acetylene flame spray unit for deposition purpose. The sample was manually held at the pre-determined stand-off distance using suitable device and the unit was switched on. The Flame was lit and the substrate was preheated to roundabout 100°C. After this the rod was fed and at the same time the compressed air jet was supplied. Special care was taken to see that there is no burn-through in the specimen due to overheating. Thus, one after another fifteen samples were sprayed.

3.2 The Characterisation Procedure of the Deposited Coating

3.2.1 Hardness Testing

After the deposition process is over the coatings were allowed to cool in air and then filed to 6mm thickness. Then the samples were taken to the hardness testing unit. The hardness of each sample was measured using a Brinell hardness testing machine. Indentation was taken on the samples using 250 kg load and 10mm dia steel ball for 60 seconds. The imprint dia were measured for each specimen and these were treated as the measures of the hardness values.

3.2.2 Metallographic Sample Preparation

In IIT the metallographic sample preparation procedure were started. The big cuts were given by carbide blade cutter and hacksaw while the fine cuts were given by diamond cutter. Extremely small pieces were cut and then mounted by cold setting compounds and cold setting liquids. The samples were then ground in low-vibratory belt grinder and then in emery grinding paper (0, 1, 2, 3, 4 respectively). After that the samples were fine polished using 0.1 micron size alumina powder. The samples were then etched using 1:1 mixture of concentrated nitric acid and glacial acetic acid [18]. The samples were thus made ready for

optical and scanning electron microscopy.

3.2.3 Light Optical Microscopy

The prepared samples were seen under the Laborlux 12 ME microscope at different magnification. some photographs were taken at 100X and 200X to reveal some important features. By point counting method volume fraction of porosity of different samples were measured under microscope. In this method, an eyepiece was chosen with graticules containing square grid. Among all the cross points twenty-five were selected. Twenty readings were taken for each sample and how many grid points out of those 25 points fall on the powder phase were counted. The standard deviation of those 20 readings was calculated and then the standard error of mean was also calculated. Then the confidence interval of the measured volume fraction at 95% confidence level was calculated using an easy formula[19].

3.2.4 Scanning Electron Microscopy

The samples were then observed under JSM 840A scanning electron microscope (JEOL) to reveal distinct microstructural features of the coating.

3.2.5 X-ray Diffraction Analysis

X-ray diffraction analysis was carried out to the 20B rod specimen before being sprayed after preparing the sample properly. The coating was made to spall off the substrate and after proper preparation it was also analysed to identify if some other phases have formed in the coating or not.

3.2.6 Electron Probe Microanalysis

To understand the constituents of different features observed from the optical and SEM studies, EPMA was done on the coating. Four different features were identified and spot

analysis was done on these features to get the compositions using the Electron Probe Microanalizer (JXA-8600). X-ray mapping was also done using the same instrument to find out how the elements are distributed throughout the structure.

3.3 Characterisation of 20B Powder

The 20B powder is found to be non-flowable and hence it cannot be sprayed using the 6P II hand held thermospray gun. Hence, detail characterisation was done on the powder to find out the possible reasons of its non-flowability. Firstly SEM photographs were taken to guess about the aspect ratio and the shape of the powder particles. Then by sieve analysis the powder was screened into mainly three different size fractions. 100, 200, and 240 BSS sized sieves were taken and the 20B powder was shaken for 40 minutes to get different size fractions. Then a flowability measurement was done on the different size fractions using an flowmeter (manufactured in Central Workshop, IIT Kanpur) with an orifice diameter of 2 mm. At last, the compositions of the most flowable size fraction of the 20B powder and the reported bulk composition of the 20B powder were compared by the quantitative analysis using XRD technique [20].

Table 3.1: The Box-Behnken Model

SL. No.	Variable(X_1)	Variable(X_2)	Variable(X_3)	Output(Y)
1	-1	-1	0	
2	-1	1	0	
3		-1	0	
4		1	0	
5		0	-1	
6	-1	0	1	
7	1	0	-1	
8	1	0	1	
9	0	-1	-1	
10	0	-1	1	
11	0	1	-1	
12	0	1	1	
13	0	0	0	
14	0	0	0	
15	0	0	0	

Table 3.2: The numerical values of different parameters used in the experiment.

Variable	Parameter Name	Low Level(-1)	Intermediate Level(0)	High Level(+1)
X_1	feed rate	0.33 cm/sec	0.38 cm/sec	0.45 cm/sec
X_2	stand-off distance	70mm	85mm	100mm
X_3	jet air pressure	2.5 kg/cm^2	3 kg/cm^2	3. 5 kg/cm^2

Table 3.3: Reported composition of the constituents of the 20B rod.

name of the Constituent	Weight Percent
Copper	(20-23)
Boron Nitride	(12-16)
Carbon	(7-10)
Nickel	Balance

Chapter 4

Results and Discussion

As mentioned in the previous chapter, two sets of experiments were done using oxy-acetylene flame spraying technique. First, I will discuss the results of process optimisation when coating are deposited using the 20B rod. Then I will discuss the results when the 20B powder of the same mesh size as the 20B rod was characterised using different techniques.

4.1 Experiments with 20B Rod

The experiments are done following the Box-Behnken model as explained before and the results are given in Table 4.1 and Table 4.2. These two tables give the raw data obtained from the hardness testing and volume fraction determination of the coating under the microscope. Three middle or centre point replicates were taken in the model to estimate the true run-to-run variability inherent in the experiment.

The goal of this experiment is to optimise the process conditions for the specification needed for these coatings. According to the specification at 4BRD Chakeri, Kanpur, the hardness of the coating should be in the range of (5-6.5) mm diameter of impression [22]. Therefore, we have done statistical analysis, as discussed in section 4.1.2, to estimate the primary and secondary effects of the experimental variables on the coatings. In order to get a better physical understanding of the process, I have characterised the 20B rod and coatings

as discussed in next section.

4.1.1 Characterisation of the Coating

1. XRD Analysis on the Coating

Figure 4.1 and Figure 4.2 are obtained from the XRD analysis of the 20B rod and the coating after the deposition. At number of 2θ-values, more than one possible elements or compounds are labelled. It is because the 2 θ- values of those elements or compounds are closely matching. A detail analysis was done on these XRD figures, the possible d-matches were found out and the possible elements or compounds are reported in Table 4.3(a) and 4.3(b). Figure 4.1 shows that the 20B rod has Ni, Cu, C, and BN peaks along with peaks of Na-silicate which is used as a binder to produce 20B rod from the powder. It looks like that, Copper and Nickel remain in the deposited coating in the form of an intermetallic Cu_3Ni_8. Presence of NiC is also observed in the XRD analysis of the 20B rod. Figure 4.2 shows almost all the features of the previous figure, except the addition of some copper oxide peaks and disappearance of the Na-silicate peaks. It seems that during the deposition process, some of the droplets are oxidised to some extent which is quite natural as the related temperature is quite high (nearing 3000°C).

Comparing Figure 4.1 and Figure 4.2, the integrated intensities of the peaks of the 20B rod and the coating are found to be quite different. this is expected since the peak intensity is a complex function of the volume fraction of various constituents of the sample. We already know from the qualitative analysis that 20B rod has Na-silicate and coating has Copper oxide as additional constituent.

2. Optical Observations of the Coating Structure

From the optical microscopy of the coating, different structural features are observed. Figure 4.3(a) and 4.3(b) show that the particles inside the coating obtained from the depo-

sition of 20B rod by flame spraying process, have undergone plastic deformation in molten or semi-molten state. Figure 4.3(c) clearly shows the interfacial region of the coating. It is observed that the droplets obtain a lenticular or splat like shape near the interface. Near the interface the droplets seem to have flown well and flattened. But, as the distance increases from the interface, the particle shape changes. It is also observed from the microstructures that the coating is porous in nature and the porosity is not evenly distributed throughout the structure.

3. Studying the structure by SEM

A detailed Scanning Electron Microscopy analysis has also been done to find out the structural features of the 20B rod coating in a better manner. In this context, it is worthwhile to mention that the roughness factor of the deposited coating is very high and hence it was very difficult to bring even a small portion of the coating into the focus at higher magnification in optical analysis. This problem was not there in SEM analysis as its depth of focus is very high. Figure 4.4(a) to 4.4(h) show SEM photographs of different samples revealing subtle features of the structure of the coating. Figure 4.4(a) and 4.4(b) show the interface of the coating. These two figures, taken at relatively lower magnification, also give a broader view of the coating structure. Figure 4.4(c) shows the droplet sizes of the coating are about 70 μm in one direction, which is in agreement with the particle size within the 20B rod different areas. Figure 4.4(d) and 4.4(e) show the internal structure of the samples showing the irregular shape of the particles. Figure 4.4(f) shows a near spherical droplet which is a rare feature in the micrographs of the coating, though it should be admitted that the actual shape of this droplet may not be spherical in 3-dimension. Figure 4.4(g) shows a distinct splat structure of a droplet attached to the substrate surface, while figure 4.4(h) reveals clearly the mechanical interlocking within the particles inside a coating. It is worthwhile to mention in this context, that mechanical interlocking seems to be the mechanism by which the particles are attached to each other and the coating gets it strength.

4. Analysis of the coating by EPMA

Electron probe microanalysis has been done on the coatings to find out the composition of different structural features inside the coating. The spot analysis results are reported in Table 4.4(a) and 4.4(b). The spot analysis was done on two samples deposited with diametrically opposite parameter combination. Analysis was done on specific microstructural features as shown in Figure 4.4(b). These microstructural features are shaded grain, large white region, dark region, and the small bright droplet. One sample was coated at low value of the feed rate and the S.O.D. keeping the C.A.P. at intermediate value while the other sample was coated at high values of the feed rate and the S.O.D. keeping the C.A.P. at intermediate level. After doing the spot analysis on different features of the coating, it is found that relatively dark areas of the microstructure are rich in carbon. The shaded gray grains are rich in nickel and copper and their ratio indicate that these may be present in the coating in the form of an intermetallic which also confirm the XRD results. Some small, bright droplets were found in the structure and the EPMA analysis shows these features to be rich in nickel. Ni-mapping, Cu-mapping, and C-mapping were also done on one structure to understand how these elements and intermetallics are distributed in the structure. These element mapping and the corresponding structure are shown in Figure 4.5(a) to 4.5(d). Analysing the cu-map and the Ni-map, it is confirmed that they are present in intermetallic form in some features as the dots on the map fall on almost the same spots. In addition to the concentrated areas of Ni and Cu they seem to be distributed throughout the sample indicating mechanical alloying during powder preparation.

4.1.2 Statistical Analysis

1. Process Characterisation

First, I wanted to find out the effect of processing parameters, the feed rate, the stand-off distance(S.O.D.), and the compressed air pressure(C.A.P.) on hardness of the coating.

For this purpose, the data from Table 4.1 is analysed using screening model. Screening model tests the influence of independent variables and their combinations on the response variables. Table 4.5(a) to 4.5(c) give results of the screening fit using the hardness data as the response variable and feed rate, S.O.D., C.A.P., feed rate * S.O.D., S.O.D. * C.A.P., and C.A.P. * feed rate as different main and interaction effects. In Table 4.5(a) summary of fit results show the numeric summaries of the response for the multiple regression model. 'Rsquare' estimates the proportion of the variation in the response around the mean that can be attributed to the effect terms in the model. 'Rsquare Adj' adjusts rsquare to make it more comparable over model with different numbers of parameters by using the degrees of freedom in its computation. 'Root Mean Square Error' (RMS error) estimates the standard deviation of the random error. 'Mean of Response is the overall mean of the response variable. In this case, 'Rsquare' value is 0.445 and the RMS error is 0.453 for the 'Mean of Response' equal to 6.95 which shows the model to be a good fit and the RMS error is also tolerable.

Tables 4.5(b) and Table 4.5(c) give the most important results of the analysis in terms of assessing the main effects and the interactions in between the parameters using the hardness values as the response. Table 4.5(b) describes the parameter estimates in the linear model and a t-test for the hypothesis that each parameter is zero. Term names the estimated parameter. The first parameter is always the intercept. Estimate lists the parameter estimates for each term. They are the coefficients of the linear model found by least squares. Std Error is an estimate of the standard deviation of the distribution of the parameter estimate. It is used to construct t tests and confidence intervals for the parameter. A test that whether the true parameter is zero or not is judged by the t-test. Analysing the results of Table 4.5(b) the size of effects are clearly understood. The S.O.D. and the feed rate seem to have large effect while C.A.P. on its own has little effect. Among the interaction terms C.A.P. * feed rate and S.O.D. * feed rate are also significant while C.A.P. * S.O.D. has small effect.

Table 4.5(c) shows the effect test which is nothing but a joint test that all the parameters

for an individual effect are zero. Ordinarily Nparm (number of parameters) and DF (degree of freedom) are the same. They are different if there are linear combinations found among the regressors such that an effect cannot be tested to its fullest extent. F ratio here is the F statistic for testing that the effect is zero. It is the ratio of the mean square for the effect divided by the mean square for error. It is observed that S.O.D. has largest effect followed by feed rate while C.A.P. has little effect. Among the interaction effects, C.A.P. * feed rate has large effect followed by moderate effect of feed rate * S.O.D.. The size of interaction of S.O.D. * C.A.P. is little compared to others. Thus, the results obtained from the effect test table (Table 4.5(c)) strengthen the observations of the parameter estimates table (Table 4.5(b)).

Table 4.6(a) to 4.6(c) represent the analysis of the effects and interactions of the parameters within the screening fit model in similar fashion as in tables of 4.5 but this time using the volume fraction data as the response variable. The tables represent the summary of fit, parameter estimates, and effect test results respectively. From Table 4.6(b) and 4.6(c), it is observed that the effect of feed rate and C.A.P. on the porosity level of the coating is significant while the effect size of S.O.D. is small. Among the interaction effects, feed rate * S.O.D. is significant while the effect of C.A.P. * feed rate and S.O.D. * C.A.P. is little.

Figure 4.6(a) and 4.6(b) show the interaction profiles for the two responses of the investigation, i.e. the hardness and the volume fraction of the coating. Interaction plots consider all the two way interactions that a system possesses. In an interaction plot, evidence of interaction shows as nonparallel lines. In figure 4.6(a) considering the hardness data as the response variable all the two way interactions between the parameters are shown. It shows S.O.D. * C.A.P. has very little interaction within themselves. among the other interactions, feed rate * S.O.D. is moderate while the size of effect for the interaction of C.A.P. * feed rate is maximum. This observation also supports the findings from the earlier parameter estimate and effect test tables. At higher values of the feed rate, the hardness of the coating

decreases with increasing C.A.P. while at the lower values of the feed rate the dependence reverses its nature. On the other hand, at higher values of the C.A.P. an increase in the feed rate decreases hardness of the coating at a brisk rate and with low value of the C.A.P. the rate at which the hardness value decreases with the feed rate decreases. The interaction of C.A.P. * S.O.D. is little as it is evident from a set of parallel lines in the interaction plot. While analysing feed rate * S.O.D. interaction, it is observed that at all values of the S.O.D., hardness value decreases with increasing feed rate but the rate of hardness decrement increases as we go to lower values of S.O.D..

In Figure 4.6(b) the volume fraction of the powder particles are taken as the response variable and then all the interactions between the parameters are shown by fitting the data into the screening fit model. The only noticeable interaction in this case is observed in case of feed rate * S.O.D.. The interaction of S.O.D. * C.A.P. is moderate but there is almost no interaction in case of C.A.P. * feed rate. At higher values of the feed rate the volume fraction of porosity remains almost the same with variation in the value of the S.O.D. while at lower values of the feed rate the porosity level increases with increasing the S.O.D.. On the other hand, an increase in the feed rate increases the porosity level of the coating at a lower value of the S.O.D.. However, the porosity level remains the same with variation in the feed rate at a higher S.O.D. value. If one sets the S.O.D. at a lower value then with an increasing C.A.P. value the porosity level of the coating falls down.

Examining all the results obtained from the statistical analysis it seems that a low value of the feed rate, a low value of the S.O.D., and a high value of the C.A.P. give rise to a coating with low porosity level and desired hardness value. Satisfactory physical explanation can also be given in support of the above statement. A low value of the feed rate allows a lesser mass of the 20B rod to be exposed in the heat at a specific period of time. Thus the droplets get enough chance to acquire more temperature and in the process flow well to fill up the voids after hitting the substrate. Associated high value of the C.A.P. helps those

molten droplets to impact on the substrate with a much more momentum and in the process helps in the formation of a well-packed coating. This seems to be the reason why the size of interaction in between the feed rate and the C.A.P. is large when hardness is used as the response variable. It is also observed that at high value of the feed rate increased C.A.P. value is contributing to lower the hardness value which is not wanted. This may be due to the presence of a larger mass of 20B rod at small time interval which means that a lot of particles will remain unmolten and high C.A.P. will carry those particle to the substrate. In the process, the particles will be loosely held and the hardness value drops down drastically. When the volume fraction response is observed there also large level of porosity is found. A lower value of the S.O.D. probably controls the temperature and the momentum of the molten droplets while these are on the way to impact on the substrate. Keeping a high value of the S.O.D. means that one is allowing the droplets to cool down and loose its momentum which will give rise to a porous coating with a low hardness value.

2. Process Optimisation

After the process characterisation, in which the size of effect of each main factor as well as the interactions between the parameters are measured for both the responses, I would like to optimise the process. I would like to get a hardness value of the coating equal to a minimum diameter of impression while the volume fraction of the powder phase to be the maximum value and the process was accordingly optimised using prediction profile within a screening fit criterion.

Figure 4.7 shows the prediction profile from the screening fit model which displays prediction traces for each X variable using the hardness and the volume fraction both as the response variables. A prediction trace is the predicted response as one variable is changed while the others are held constant at the current values. The vertical red line for each X variable shows its current value or current setting. If the X variable is discrete, the trace displays five predicted values. The horizontal green line shows the current predicted value of

each response variable for the current value of the X variables. The 95% confidence interval for the predicted values is shown by error bars above and below each marker. Prediction profiles are especially useful in multiple response models to help judge which factor values can optimise a complex set of criteria. Desirability function is chosen and added to the prediction profile. It helps one to set the desired response values and then optimise the process according to the given responses with respect to its parameters. In this case, I have tried to achieve such parameter combination so that the hardness response is minimum while the volume fraction of the powder phase is the maximum. Accordingly the desirability settings are done and then the screening model is run. The vertical lines are altered in such a manner so as the desirability traces at the bottom of the figure decrease everywhere except the current values of the effects. This indicates that any further adjustment could decrease the overall desirability. In this case, to achieve that criteria for the desirability traces, the physical values of the three parameters used in the experiments are calculated. These are reported in Table 4.7.

From the prediction profile it can be said that feed rate of the 20B rod should be closely controlled as it seems to affect hardness of the coating largely. A careful control of C.A.P. is also needed while wide tolerance in S.O.D. is observed when hardness is used as the response variable. On the other hand, the porosity level of the coating seems to be almost equally affected by all the process parameters. Altogether, keeping all the interactions in between the parameters in mind, it can be said that a low value of the feed rate and a low value of the S.O.D. gives a coating with a low porosity level if the C.A.P. is maintained at a higher value.

3. Hardness Versus Volume Fraction

Not much literature exist about correlation of the hardness property with the microstructure of the coating. In this study, we can correlate hardness with porosity for the coating made by oxy-acetylene flame spraying of the 20B rod as shown in Figure 4.8. In the fig-

shown how hardness is related to the volume fraction of the powder phase of the coating. It is observed that we can get a coating with hardness value equal to 6.5 mm diameter of impression with a porosity level varying from (15-35)%. Thus it can be said that hardness of the coating is not only a function of porosity only but it is a function of the particle nature also. The nature of the droplets, when they impact on the substrate, also determines the hardness of the coating, in a large way. Particle temperature and particle momentum seem to be the crucial factors that determine the hardness of the coating as the amount of plastic deformation of the particles depends on these two factors. However, in the process optimisation, I have shown that we can get a coating of only 20% porosity while limiting its hardness within 6.5 mm diameter of impression maintaining the process parameters at the values mentioned in Table 4.7.

4.2 Characterisation of 20B powder

Attempts were made to deposit 20B powder directly on to the steel substrate under specific parameter combinations. METCO 6P-II Hand Held Thermospray Gun was used to deposit the 20B powder. However, the 20B powder could not be spraye d as the powder seemed to be not flowable at all. After several trials, the nozzle tip of the gun was blocked by the powder and then blasted. For these reasons, I did many experiments to find out the possible reasons of its non-flowability.

The 20B powder was first screened using sieve shaker and then the flowability of each size fraction was measured. The results of the tests are reported in Table 4.8(a), 4.8(b), and 4.9. Table 4.8(b) shows that a large percentag e of the powder is of -240 BSS while only a small percentage of it is +200 BSS size. Table 4.9 shows the measurement of the flowability of each size fraction of the powder. It is clear that the 20B powder of the size range in between -200 BSS and +240 BSS is by far the most flowable size fraction. It takes much lesser time to flow compared to the +200 BSS size fraction. 20B powder of the size range

(-200 to +240) BSS constitute 45% of the total weight and this fraction is relatively flowable. It is revealed from the SEM photograph of the 20B powder (Figure 4.9(a) and 4.9(b)) that the powder particles are irregular in shape and have high aspect ratio. In general, if the particle shape is irregular and the size is fine then they are less flowable. In addition to that, presence of ultrafine particles alter the flow characteristics of an otherwise flowa ble powder [21]. In our case, a large fraction of powder particles (nearly 50%) was -240 BSS with flowability nil and these along with the shape of the powder seem to make the 20B powder non-flowable.

Hence, it seems that by changing the particle size distribution, it should be possible to deposit coatings by using 20B powder in the size range of (-200 to +240) BSS. However, it is necessary to make sure that overall powder composition does not change by selecting powder with specific mesh size. In other words, chemical composition is homogeneous with respect to the particle size.

Quantitative analysis was done on the +240 BSS size fraction of the 20B powder using the XRD technique (procedure mentioned in chapter 3). XRD patterns for the 20B powder and its +240 BSS size fraction are shown in Figure 4.10 and 4.11. The analysis shows that the 20B powder is not chemically homogeneous with respect to the particle size. The Ni : Cu : C ratio in this size fraction is 41 : 18 : 29 which is largely different than the reported composition of the 20B powder. The result of the composition analysis is reported in Table 4.10.

The morphology, shape, and the size of the particles determine the flowability of a powder [23]. I have shown that flowability can be improved by changing the size distribution, but care should be taken to maintain the desired composition of the coating. Nevertheless, attempts will be made to deposit the 20B powder with a size range (-200 to +240) BSS.

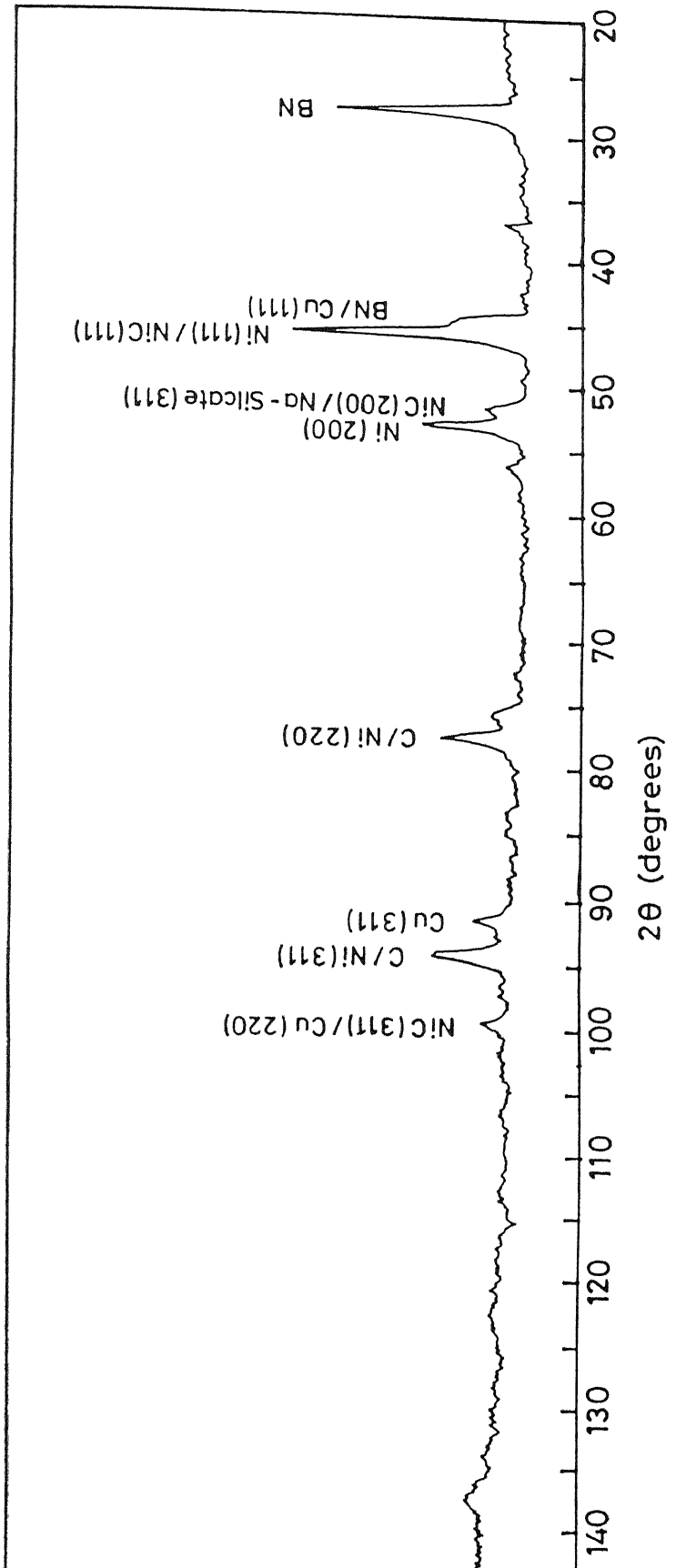

Figure 4.1 XRD pattern showing the peak positions and intensities obtained from the 20B rod.

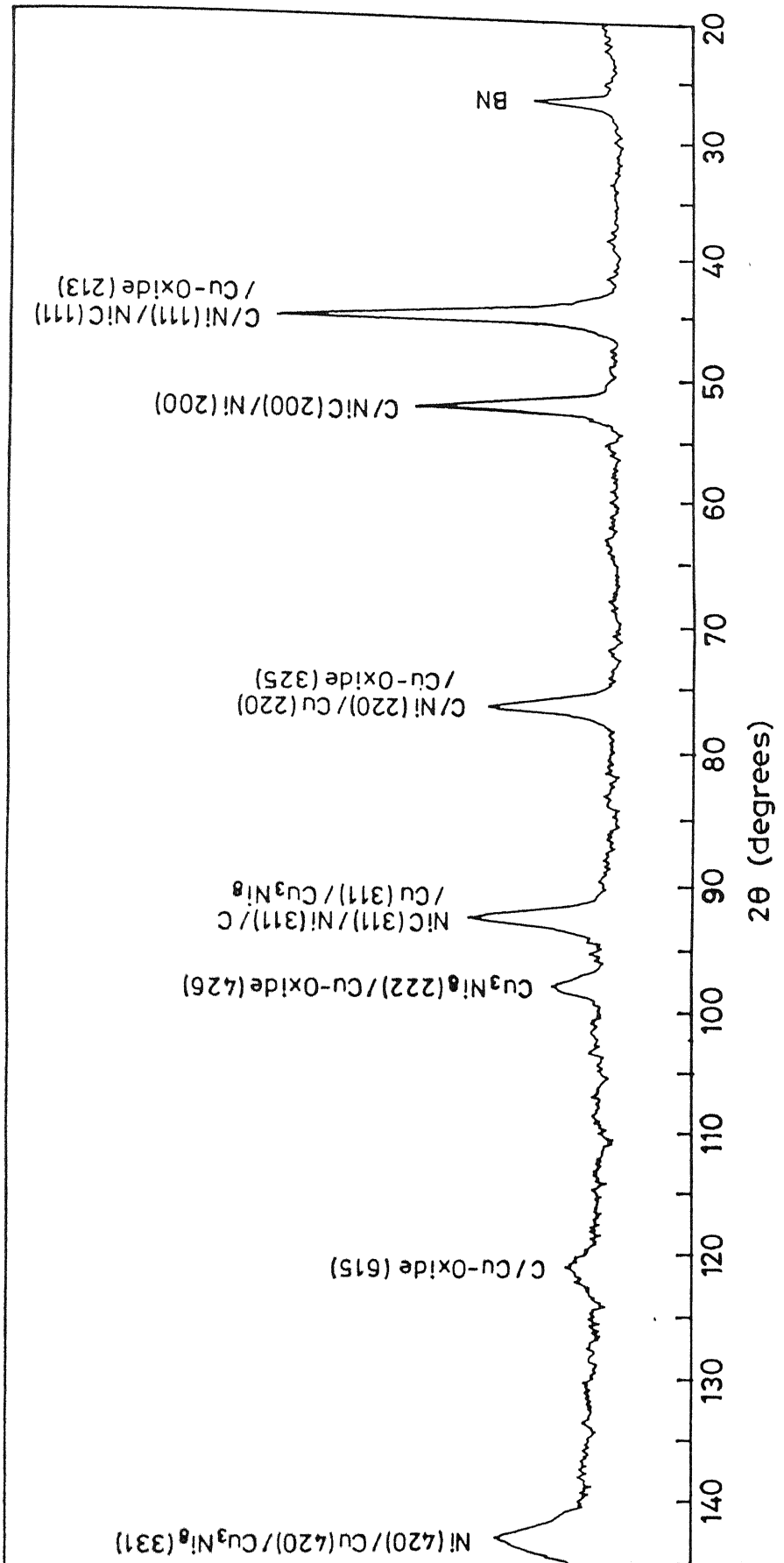

Figure 4.2 XRD pattern showing the peak positions and intensities obtained from the coating deposited by 20B rod and oxy-acetylene flame spraying.

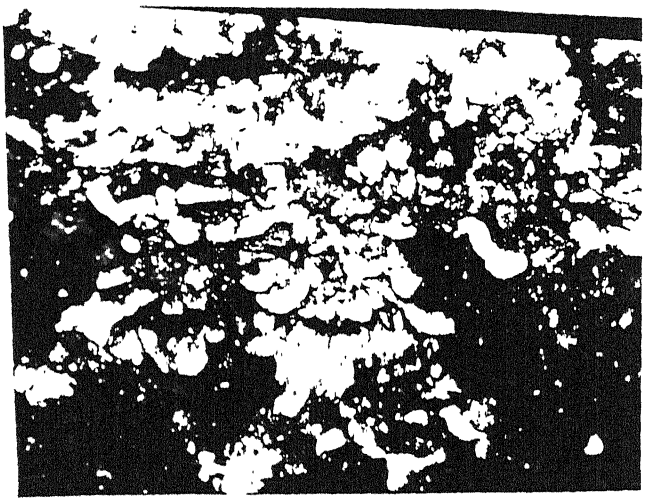

(a)

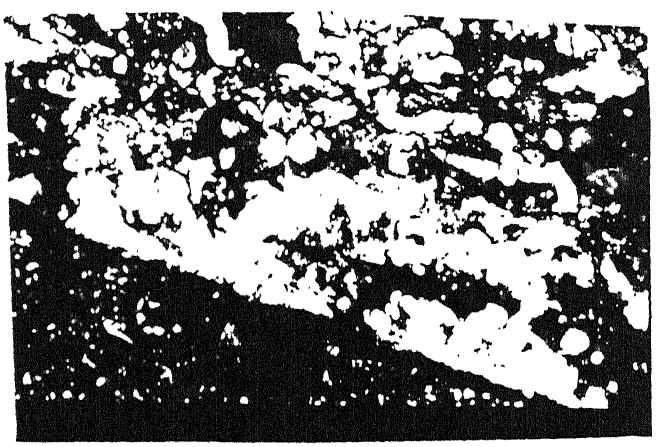

(b)

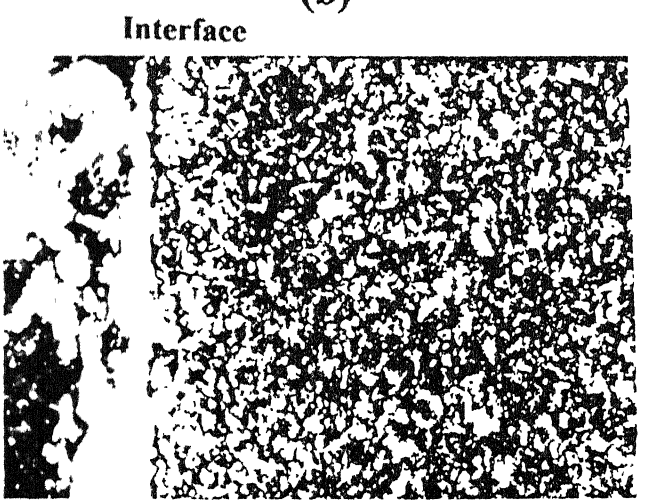

(c)

Figure 4.3 (a – c) optical micrographs of the 20 B rod coated samples showing the interface region and porosity distribution within the structure (each at 100X).

Interface

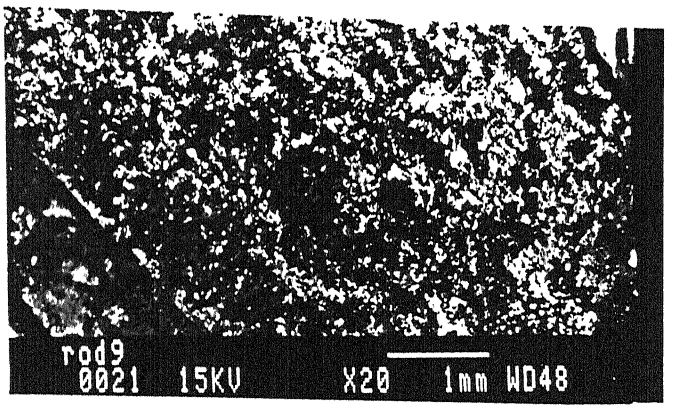

(a)

Interface

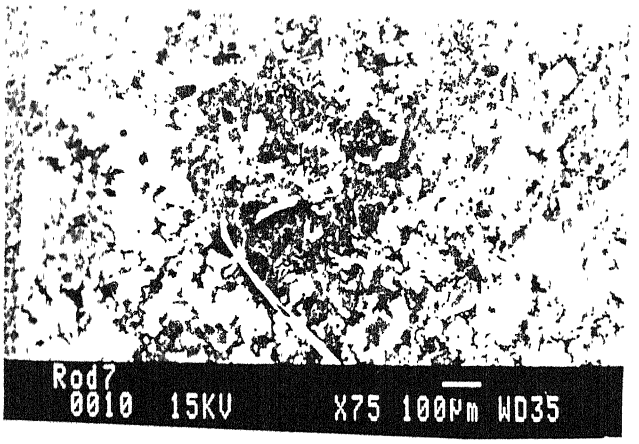

(b)

Figure 4.4 (a – h) SEM photographs of different 20B rod coated samples showing many subtle features of the microstructure at different magnification.

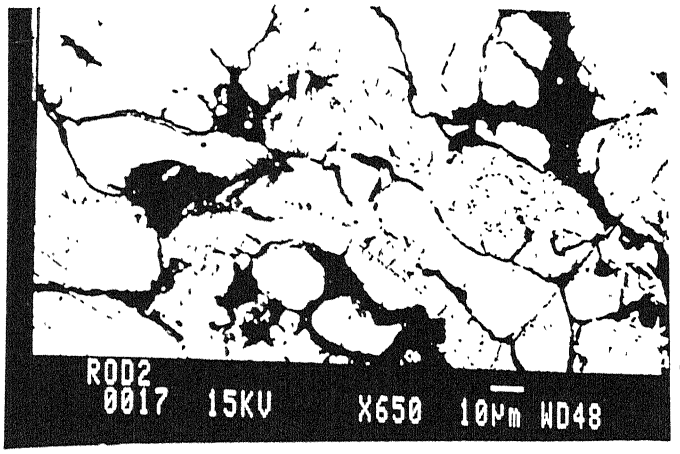
ROD2
0017 15KV X650 10µm WD48

(c)

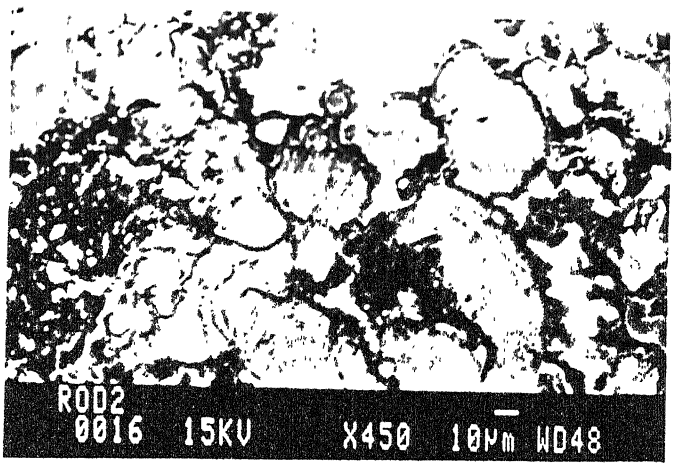
ROD2
0016 15KV X450 10µm WD48

(d)

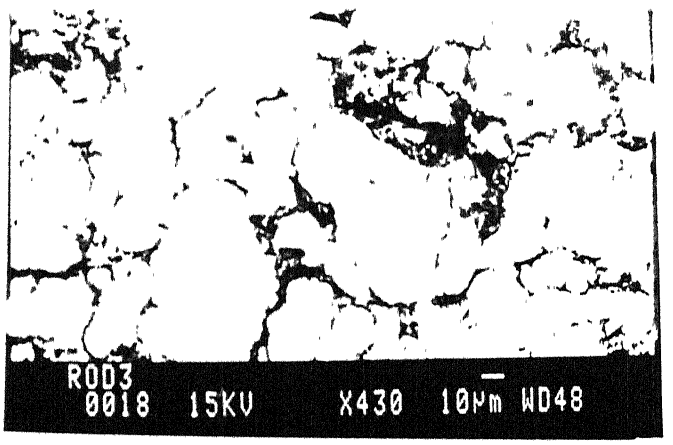
ROD3
0018 15KV X430 10µm WD48

(e)

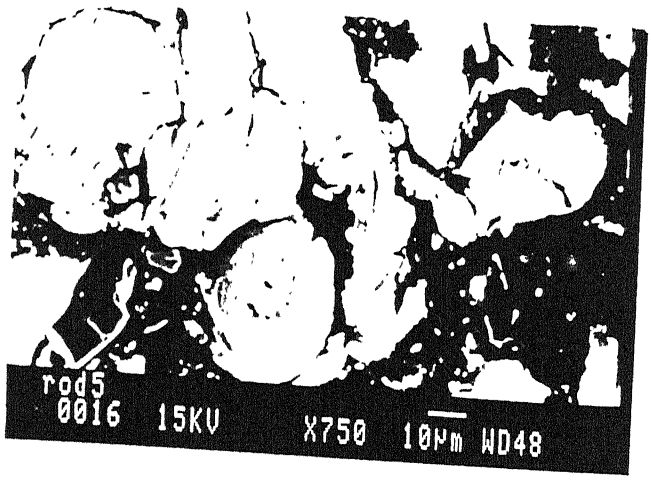

(f)

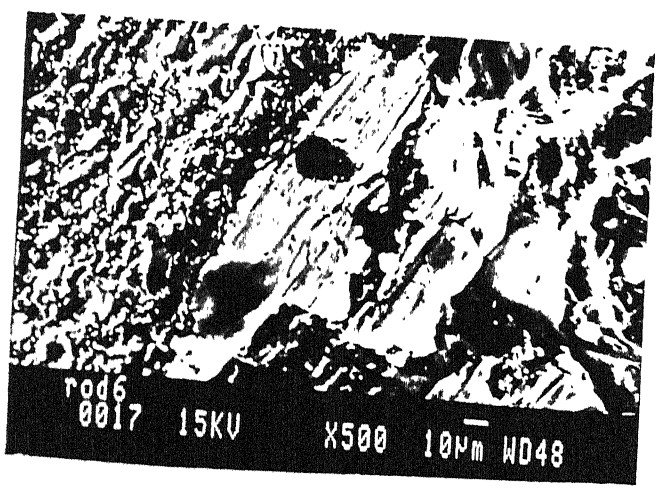

(g)

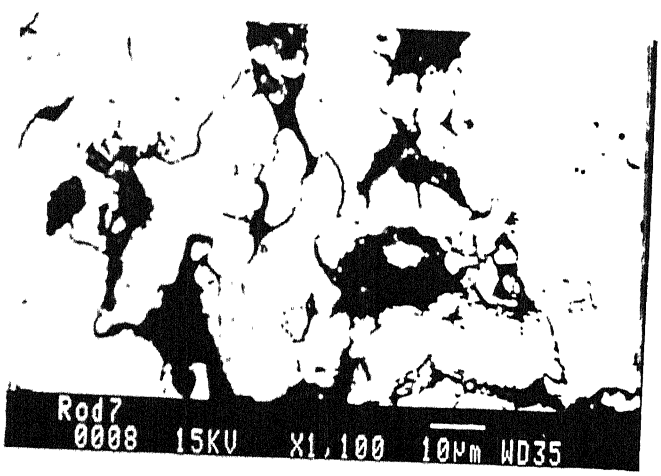

(h)

Continued

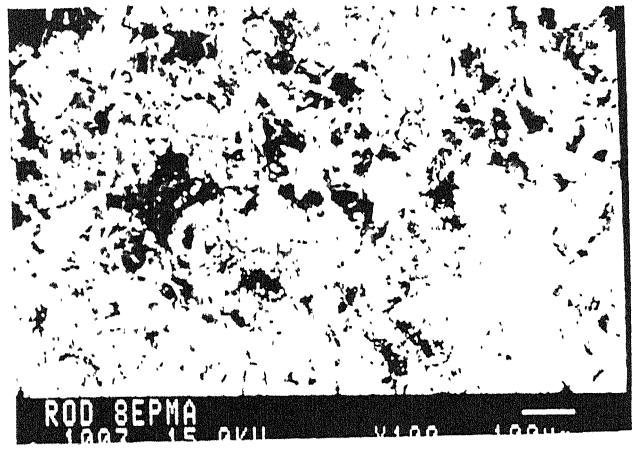

(a)

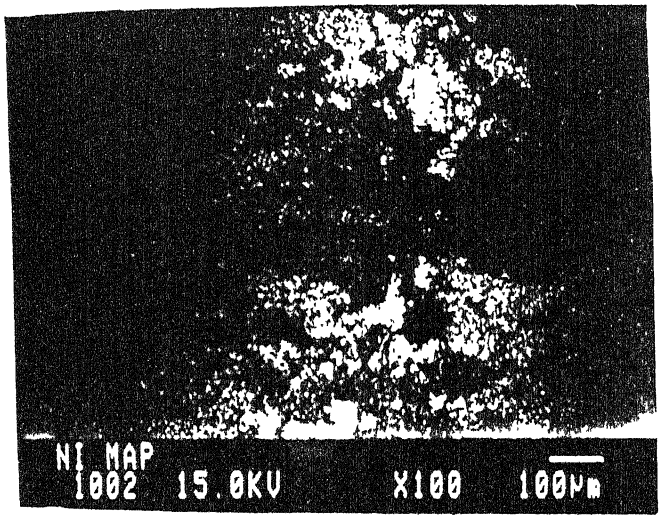

(b)

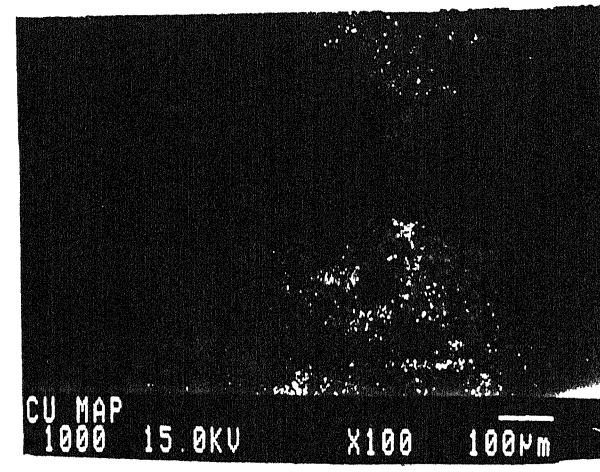

(c)

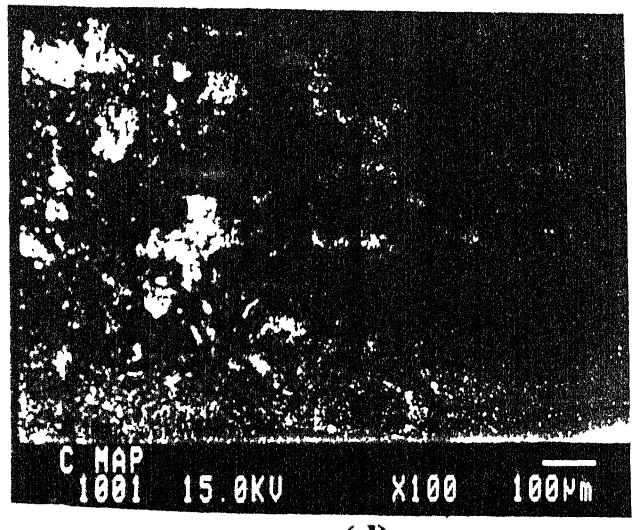

(d)

Figure 4.5 EPMA photographs showing (a) the microstructure of a 20B rod coated sample and (b – d) showing the Cu, Ni and C-map for the same microstructure at 100X.

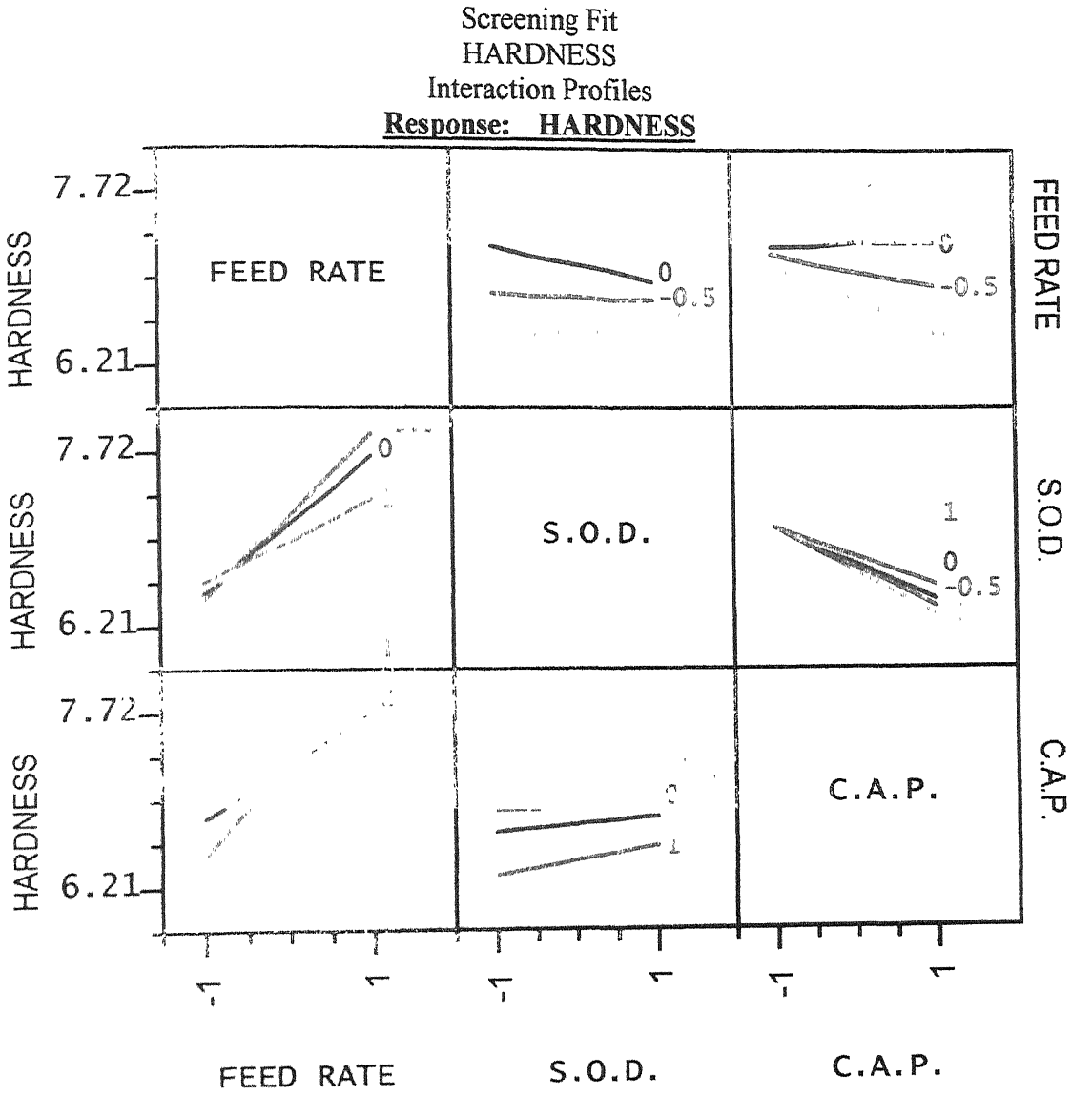

(a)

Figure 4.6 . Interaction profiles between the parameters while (a) hardness (b) volume fraction are used as the response variables.

Screening Fit
VOL.FRAC.
Interaction Profiles
Response: VOL.FRAC.

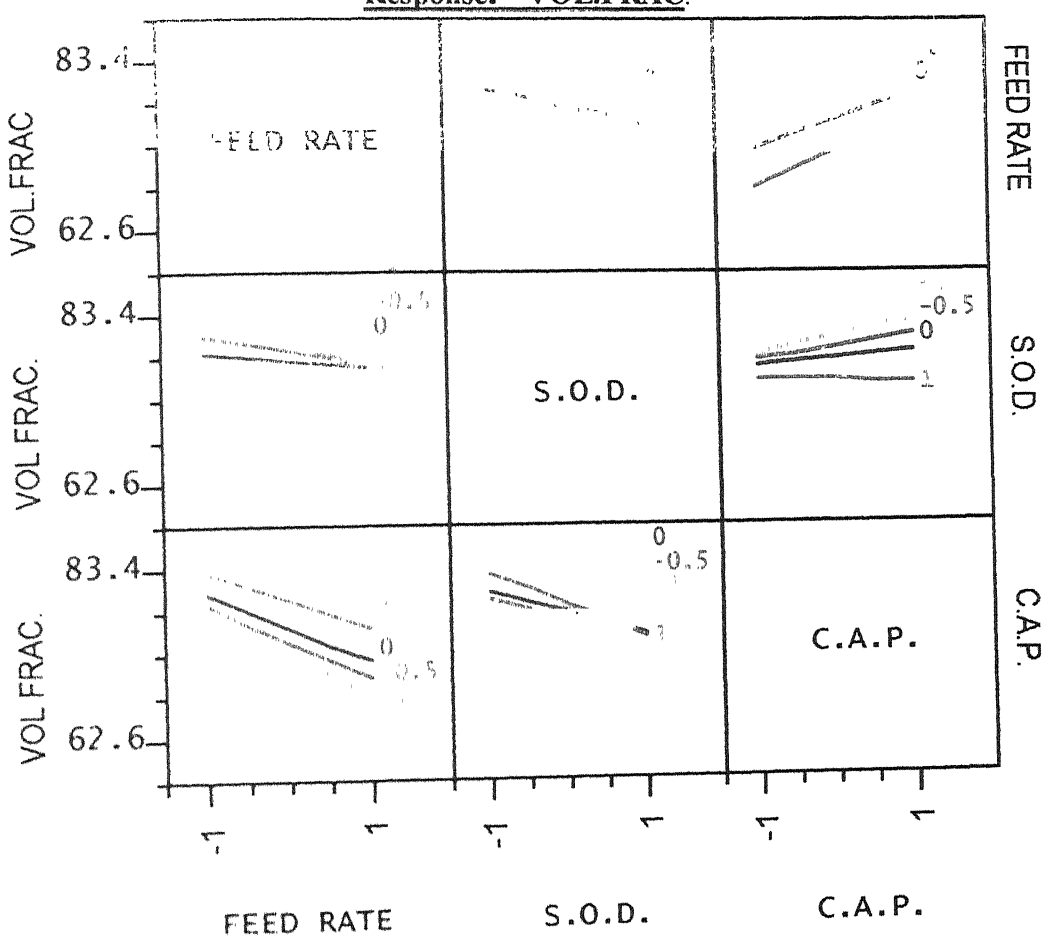

(b)

Screening Fit
HARDNESS
VOL.FRAC.

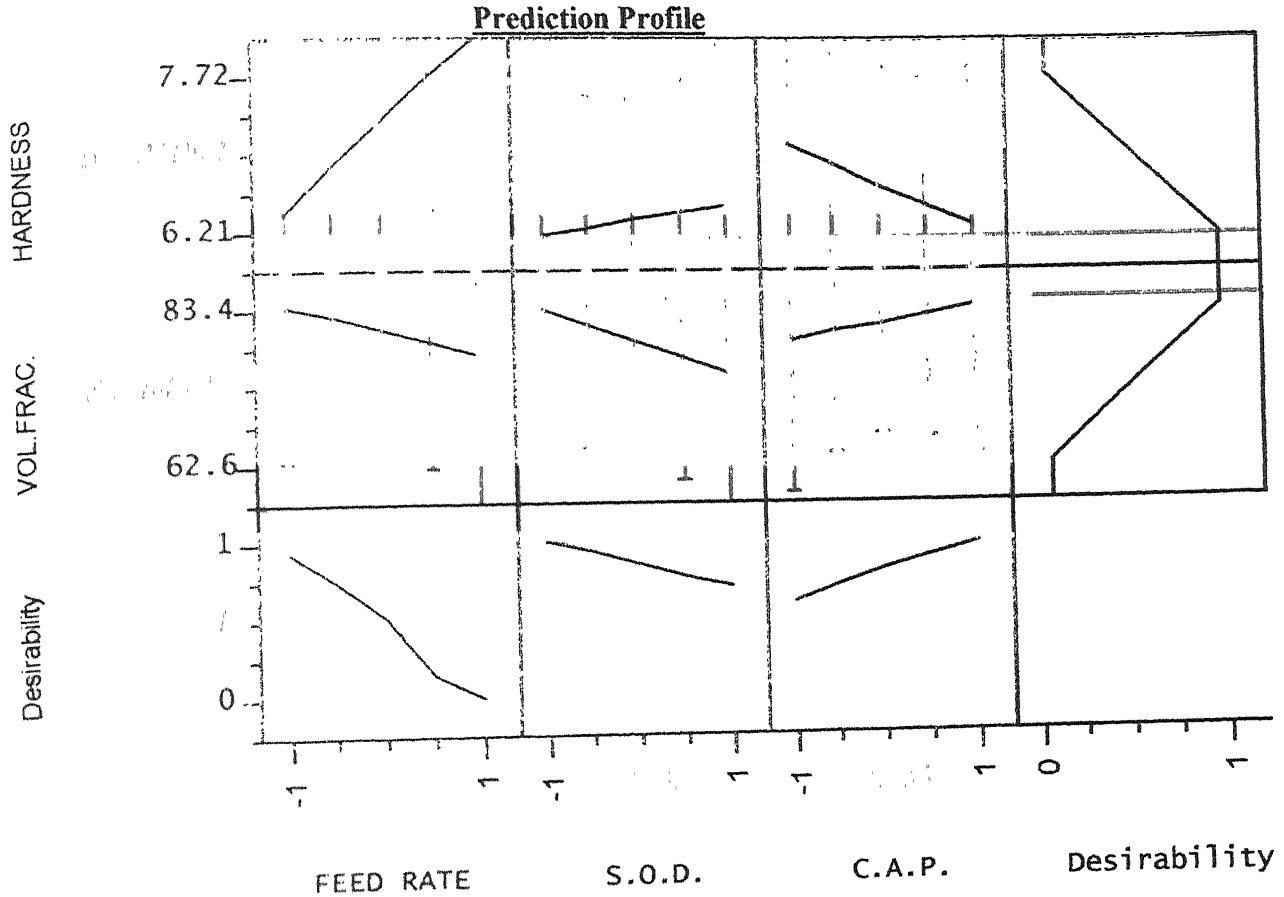

Figure 4.7 Prediction profile showing the current settings which optimise a desired set of response variables according to Screening Fit Model.

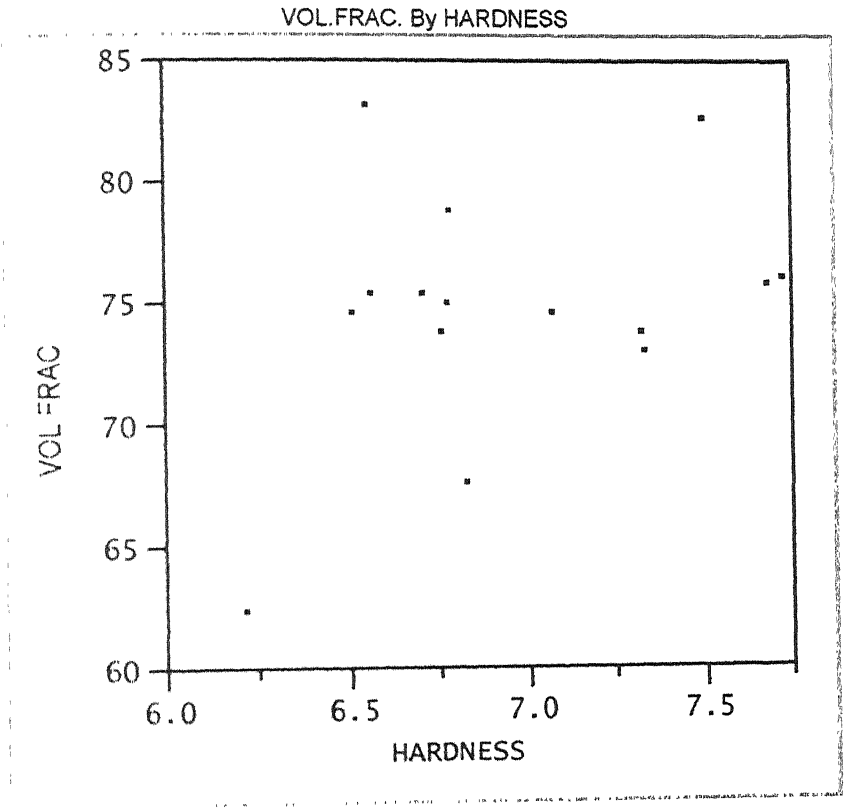

Figure 4.8 : Hardness versus volume fraction of the powder phase drawn after collecting the data from Table 4.1 and 4.2.

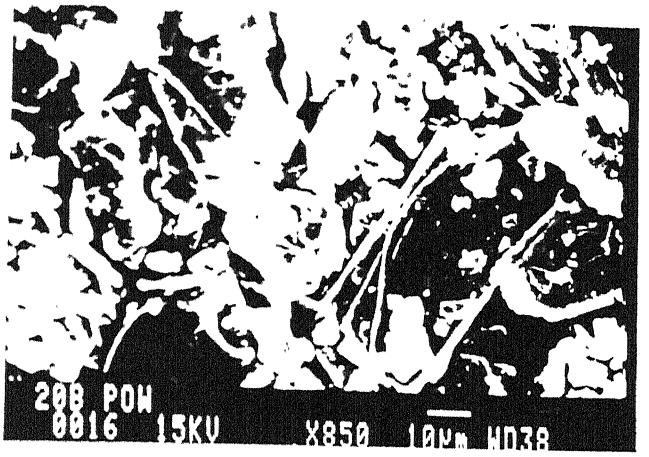

(a)

(b)

Figure 4.9 (a b) SEM photographs of 20B powder at different magnification.

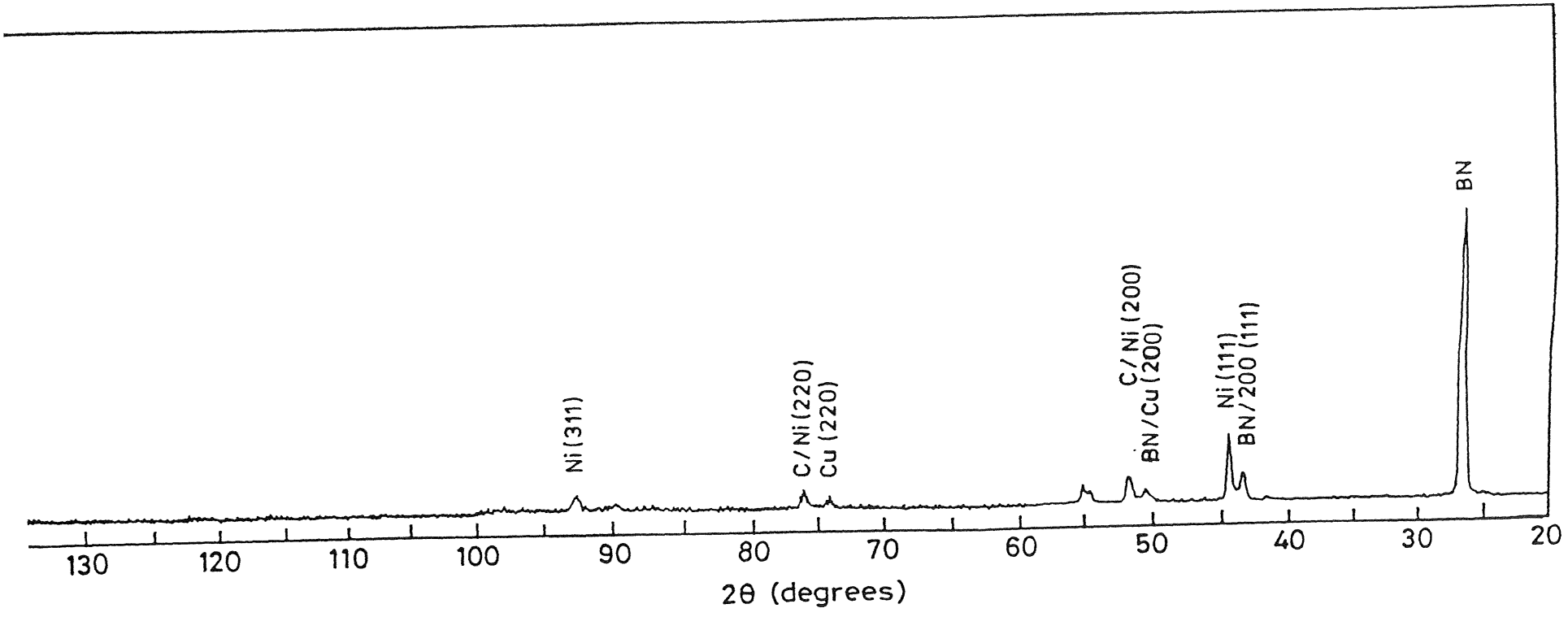

Figure 4.10 XRD pattern of 20B powder.

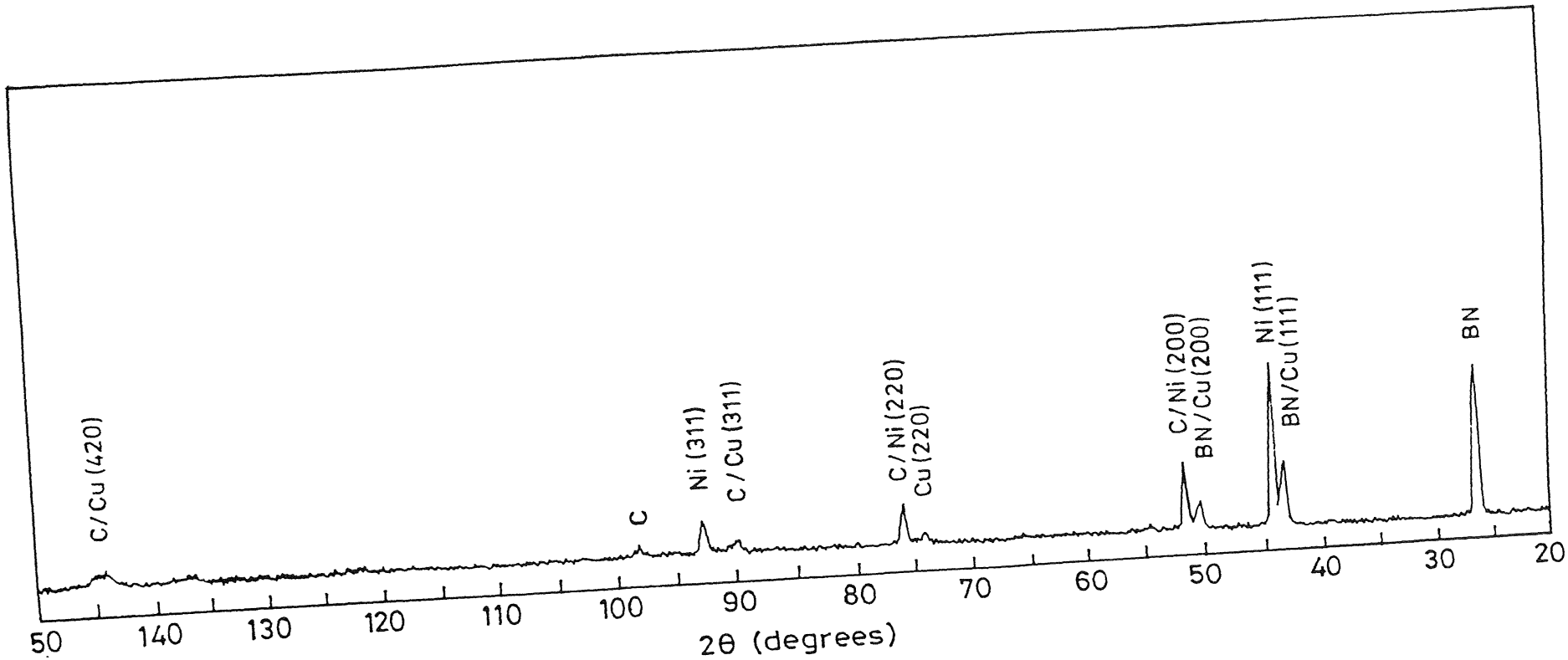

Figure 4.11 XRD pattern of 20B powder of size range (-200 to +240) Bss.

SL. No.	Feed Rate	S.O.D.	C.A.P.	HARDNESS (impression dia in mm)
1	-1	-1	0	6.55
2	-1	1	0	6.51
3	1	-1	0	7.68
4	1	1	0	6.75
5	-1	0	-1	6.82
6	-1	0	1	6.70
7	1	0	-1	6.21
8	1	0	1	7.33
9	0	-1	-1	7.32
10	0	-1	1	7.07
11	0	1	-1	6.78
12	0	1	1	6.77
13	0	0	0	7.72
14	0	0	0	7.50
15	0	0	0	6.56

Table 4.1: Raw data for the hardness testing results following The Box-Behnken Model

SL. No.	Feed Rate	S.O.D.	C.A.P.	Volume Fraction (in wt%)
1	-1	-1	0	83.40
2	-1	1	0	74.80
3	1	-1	0	76.00
4	1	1	0	74.00
5	-1	0	-1	67.80
6	-1	0	1	75.60
7	1	0	-1	62.60
8	1	0	1	73.20
9	0	-1	-1	74.00
10	0	-1	1	74.80
11	0	1	-1	79.00
12	0	1	1	75.20
13	0	0	0	75.60
14	0	0	0	82.80
15	0	0	0	76.20

Table 4.2: Raw data for the volume fraction analysis following The Box-Behnken Model

(a)

unknown d-spacing	Ni	Cu	BN	C	Na-Silicate	Ni-Oxide	Cu-Oxide	NiC	Cu_3Ni_8
3.336	x	x	v	x	x	x	x	x	x
2.083	x	v	v	x	x	x	x	x	v
2.065	x	x	v	v	x	x	x	x	x
2.034	v	x	x	x	x	x	x	v	x
1.807	x	x	v	v	v	x	x	v	v
1.766	v	x	x	x	x	x	x	v	x
1.247	v	x	x	v	x	x	x	v	v
1.086	x	v	x	v	x	x	x	x	v
1.063	v	x	x	x	x	x	x	x	v
1.018	v	v	x	v	x	x	x	v	v
0.807	v	v	x	v	x	x	x	v	v

(b)

Unknown d-spacing	Ni	Cu	BN	C	Na-Silicate	Ni-Oxide	Cu-Oxide	NiC	Cu_3Ni_8
3.336	x	x	v	x	x	x	x	x	x
2.045	v	x	x	v	x	v	v	v	v
1.773	v	x	x	v	x	v	x	v	x
1.250	v	v	x	v	x	x	v	v	x
1.068	v	v	x	v	x	x	x	x	v
1.023	v	x	x	x	x	x	v	x	v
0.885	x	x	x	v	x	x	v	x	x
0.812	v	v	x	v	x	x	x	x	v

Table 4.3: XRD analysis results for (a) 20B rod and (b) 20B rod coated sample showing possible matches for d-spacing of different elements, compounds, and intermetallics.

(a)

SL. No.	Feature in the Structure	Ni	Cu	C	BN
1	shaded grains	65.44	34.1	0.45	-
2	shaded grains	76.85	22.23	0.912	-
3	dark regions	42.92	1.17	54.75	1.13
4	dark regions	37.44	10.77	51.78	-
5	large white regions	75.91	24.08	-	-
6	large white regions	76.61	18.49	4.88	-
7	small bright droplets	81.68	18.31	-	-
8	small bright droplets	73.35	26.64	-	-

(b)

SL. No.	Feature in the Structure	Ni	Cu	C	BN
1	shaded grains	77.26	19.95	0.31	2.46
2	shaded grains	63.75	35.07	0.57	0.6
3	dark regions	10.18	11.46	70.62	7.71
4	dark regions	2.54	1.29	96.16	-
5	large white regions	35.71	13.83	50.45	-
6	large white regions	70.86	19.64	8.12	1.08
7	small bright droplets	94.97	3.91	1.11	-
8	small bright droplets	80.54	16.57	1.34	0.65

Table 4.4: EPMA results for spot analysis of (a) sample 8 and (b) sample 10 showing the compositions of the 20B rod sprayed coating. Compositions are reported in weight percent.

Screening Fit
HARDNESS

(a)

Summary of Fit

RSquare	0.445001
RSquare Adj	0.028751
Root Mean Square Error	0.453
Mean of Response	6.951333
Observations (or Sum Wgts)	15

(b)

Parameter Estimates

Term	Estimate	Std Error	t Ratio	Prob>|t|
Intercept	6.9513333	0.116964	59.43	<.0001
FEED RATE	0.17375	0.16016	1.08	0.3096
S.O.D.	-0.22625	0.16016	-1.41	0.1955
C.A.P.	0.09250.	0.16016	0.58	0.5795
FEED RAT*S.O.D.	-0.22250	0.22650	-0.98	0.3547
S.O.D.*C.A.P.	0.06	0.2265	0.26	0.7978
C.A.P.*FEED RAT	0.31	0.2265	1.37	0.2083

(c)

Effect Test

Source	Nparm	DF	Sum of Squares	F Ratio	Prob>F
FEED RATE	1	1	0.24151250	1.1769	0.3096
S.O.D.	1	1	0.40951250	1.9956	0.1955
C.A.P.	1	1	0.06845000	0.3336	0.5795
FEED RATE*S.O.D.	1	1	0.19802500	0.9650	0.3547
S.O.D.*C.A.P.	1	1	0.01440000	0.0702	0.7978
C.A.P.*FEED RATE	1	1	0.38440000	1.8732	0.2083

Table 4.5: (a) Summary of fit (b) Parameter estimates (c) Effect test results using the hardness data as the response variable.

VOL.FRAC.

(a)

Summary of Fit

RSquare	0.227844
RSquare Adj	-0.35127
Root Mean Square Error	5.907093
Mean of Response	75
Observations (or Sum Wgts)	15

(b)

Parameter Estimates

Term	Estimate	Std Error	t Ratio	Prob>|t|
Intercept	75	1.525205	49.17	<.0001
FEED RATE	-1.975	2.088473	-0.95	0.3720
S.O.D.	-0.65	2.088473	-0.31	0.7636
C.A.P.	1.925	2.088473	0.92	0.3836
FEED RAT*S.O.D.	1.65	2.953547	0.56	0.5917
S.O.D*C.A.P.	-1.15	2.953547	-0.39	0.7072
C.A.P*FEED RAT	0.7	2.953547	0.24	0.8186

(c)

Effect Test

Source	Nparm	DF	Sum of Squares	F Ratio	Prob>F
FEED RATE	1	1	31.205000	0.8943	0.3720
S.O.D.	1	1	3.380000	0.0969	0.7636
C.A.P.	1	1	29.645000	0.8496	0.3836
FEED RATE*S.O.D.	1	1	10.890000	0.3121	0.5917
S.O.D*C.A.P.	1	1	5.290000	0.1516	0.7072
C.A.P*FEED RATE	1	1	1.960000	0.0562	0.8186

Table 4.6: (a) Summary of fit (b) Parameter estimates (c) Effect test results using the volume fraction data as the response variable.

SL. No.	The Name of the Parameter	The Current Setting	The Physical Value
1	Feed Rate	-1.29	0.26 cm/sec
2	S.O.D.	-1.32	53.0 mm
3	C.A.P.	1.35	4.73 kg/cm^2

Table 4.7: The parameter settings found from statistical analysis of the results that optimises the responses.

Size(in BSS)	Equivalent Mesh Opening Size(in μm)
100	152
200	76
240	66

Size (in BSS)	Weight (in g)	Weight Fraction
+100	-	-
-100 to +200	24.5	8.2
-200 to +240	135	45
-240	140	46.67

Table 4.8: (a) The relationship between the British Standard Sieve number and the equivalent mesh opening size (b) the weight fractions obtained after sieve analysis of 20B powder.

Size (in BSS)	Flow Rate (s/ 50g)
+200	42.9
+240	29.75
-240	-

Table 4.9: Flowability measurement data for different size fractions of 20B powder

Name of the Material	Cu	BN	C	Ni
Reported 20B Powder	(20-23)	(12-16)	(7-10)	Balance
As Measured 20B powder	18.2	14	20.4	Balance
+240 BSS Size Fraction	17.6	14	28.9	40.6

Table 4.10: Comparison between the reported composition (in wt%) of the 20B powder and the measured composition of bulk 20B powder and the +240 BSS size fraction.

Chapter 5

Conclusions

The main conclusions that can be drawn regarding the oxy-acetylene flame sprayed coating using the 20B rod are given below :

5.1 Experiments with 20B Rod

5.1.1 Characterisation of the Coating

- The coatings produced by the 20B rod flame spraying on steel substrates are porous in nature and the porosity range is about (15-35)%.

- Near the interface the droplets have obtained the splat-like structure but as the distance from the interface increases the droplets do not flatten to that extent.

- There is little degree of oxidation of the molten droplets during the deposition process. The associated high degree of temperature seems to be the cause of oxidation.

- In the coating, presence of an intermetallic of nickel and copper is observed. XRD analysis shows that along with pure nickel and copper the intermetallic of these two elements is also present.

- The coating is not chemically homogeneous in terms of its constituents. EPMA analysis confirms this point by indicating different chemical composition at different features of the coating.

5.1.2 Process Characterisation

- After statistical studies of the obtained results according to Box-Behnke n model it is found that S.O.D. and feed rate have large effect on hardness value of the coating while C.A.P. has nominal effect. Among the interaction effects, C.A.P. * feed rate and feed rate * S.O.D. have large effect while S.O.D. * C.A.P. has nominal effect size.

- When volume fraction of the powder phase of the coating is used as the response variable, feed rate and C.A.P. have large effect while the effect of S.O.D. seems to be nominal. Among the interaction effects, feed rate * S.O.D. has large effect while C.A.P. * feed rate and S.O.D. * C.A.P. have nominal effects.

- The hardness is an important mechanical property for the abradable coatings and it should be controlled within specific values to meet the desired service criteria. Therefore, it is important to know the process parameters that should be controlled carefully to provide coatings with specific hardness. Based on the screening fit model, feed rate and C.A.P. should be carefully controlled to get a specific hardness for the coating

while S.O.D. can have wider range of values (Figure 4.7).

5.1.3 Process Optimisation

- The process is optimised in terms of the desired hardness and porosity level. In this case, hardness is maximised and porosity is minimised (volume fraction of powder phase is maximised). The prediction profile shows that the coating will be optimised in terms of its desired responses, if the feed rate and the S.O.D. are kept at low level and the associated C.A.P. is kept at high level of the parameter space considered.

5.2 Characterisation of the 20B Powder

- The 20B powder, as-purchased, could not be spray deposited as it was not flowable.

- After screening the powder, the flowability was improved by narrowing the size range.

- The (-200 to +240) BSS size fraction of the 20B powder did not have the same chemical composition as the as-purchased 20B powder.

Chapter 6

Suggestions for Future Work

The following things can be done to carry this work further :

- Arrangements can be made to use the oxygen/acetylene ratio as a parameter of the process and try to analyse its significance on the responses. In this study I could not try this due to the limitation of the experimental set-up at 4BRD, Chakeri.

- One can try to measure other mechanical and physical properties of the coating that are of significance and try to use those as the response variable. Many important mechanical properties like the wear resistance and the bond strength of the coatings can be tested and the effect of the processing parameters on those properties can be studied.

- One can try to characterise and optimise the process in a wider process window.

- Efforts can be made to process the 20B powder in such a manner so that a narrow size range of the particles is maintained to improve flowability. After making the 20B powder free-flowing, one can try to deposit a coating by the powder directly using planned parameter combinations and then compare the coating properties with the

20B rod coating. Thus a comparative study between the two processes can be made.

- Although the powder processed after screening is of different chemical composition, still one can verify the feasibility of depositing coatings using it.
- With the help of the data collected in this study, one can build better process models theoritically. Unlike other fields of engineering, sophisticated models are yet to be developed for combustion flame spraying process.

Appendix A

04-0850 Wavelength= 1.54056

Ni

Nickel

Nickel, syn

Rad CuKa1 λ 1.5405 Filter Ni Beta.M d-sp

Cut off: Int Diffract I/Icor

Ref: Swanson, Tatge, Natl Bur. Stand. (U.S.), Circ 539, I, 13 (1953)

Sys Cubic S.G: Fm3m (225)

a 3.5238 b c. A C

α. β γ. Z 4 mp

Ref Ibid

Dx. 8.911 Dm: SS/FOM. F 8=87(.0115, 8)

d A	Int	h	k	l
2.03400	100	1	1	1
1.76200	42	2	0	0
1.24600	21	2	2	0
1.06240	20	3	1	1
1.01720	7	2	2	2
.881000	4	4	0	0
.808400	14	3	3	1
.788000	15	4	2	0

01-1242 Wavelength= 1.54056

Cu

Copper

Rad MoKa λ: 0.709 Filter: d-sp:

Cut off: Int: I/Icor.:

Ref: Davey, Phys Rev., 25, 753 (1925)

Sys.: Cubic S.G: Fm3m (225)

a 3.597 b: c: A: C

α: β. γ: Z. 4 mp:

Ref. Dana's System of Mineralogy, 7th Ed.

Dx: 9.069 Dm: 9.010 SS/FOM: F 9=7(.174, 8)

d A	Int	h	k	l
2.08000	100	1	1	1
1.80000	86	2	0	0
1.27000	71	2	2	0
1.08000	86	3	1	1
1.04000	56	2	2	2
900000	29	4	0	0
830000	56	3	3	1
.810000	42	4	2	0
740000	42	4	2	2

45-0895 Wavelength= 1.54056

BN

Boron Nitride

d Å	Int	h	k	l
3.33000	100			
2.17000	7			
2.07000	23			
1.82000	6			
1.67000	6			
1.55000	5			
1.32000	1			
1.25000	2			

Rad λ Filter d-sp

Cut off. Int I/Icor

Ref: Danilenko, V. et al., Sov. Phys. Crystallogr. (Engl. Transl.), 26, 191 (1981)

Sys: S.G:

a b c. A C

α β γ Z mp

Ref.

Dx. Dm SS/FOM F =<1(,)

43-1104 Wavelength= 1.5405

C

Carbon

d Å	Int	h	k	l
2.06000	100			
1.78000	100			
1.26000	100			
1.07000	100			
1.04000	50			
.898000	20			
.818000	20			
.796000	50			
.726000	50			
.683000	50			

Rad Elec λ Filter: d-sp

Cut off Int: Estimation I/Icor:

Ref: Hirai, H., Kondo, K., Proc. Jpn. Acad., Ser. B, 67, 22 (1991)

Sys: S.G:

a b c: A C

α: β γ: Z: mp:

Ref.

Dx: Dm. SS/FOM. F =<1(,)

14-0020 Wavelength= 1.54056

NiC

Nickel Carbide

d Å	Int	h	k	l
2.03900	100	1	1	1
1.76500	80	2	0	0
1.25900	60			
1.06700	60	3	1	1
1.02000	40	2	2	2
.883000	20	4	0	0
.811900	60	3	3	1

Rad λ. Filter. d-sp 114.6

Cut off. Int.: I/Icor:

Ref: Pugh, Lees, Bland, Nature (London), 191, 865 (1961)

Sys: Cubic S.G:

a 3.539 b. c: A: C

α: β: γ. Z: mp:

Ref: Ibid.

Dx: Dm. SS/FOM: F_6=3(.143, 17)

39-0382 — Wavelength= 1.54056

Na2Si4O9

Sodium Silicate

Ertixite

Rad: FeKa λ: 1.9373 Filter: d-sp: Debye-Scherrer

Cut off: Int: Estimation: I/Icor:

Ref: Zhang, R., Han, F., Du, C., Zhongnan Kuangye Xueyuan Xuebao, 1, 43 (1986)

Sys: Cubic S.G: Pa3 (205)

a: 5.975 b: c: A: C:

α: β: γ: Z: 1 mp:

Ref: Ibid

Dx: 2.353 Dm: 2.350 SS/FOM: F_9=12(.068, 11)

d Å	Int	h	k	l
3.44300	20	1	1	1
2.98800	20	2	0	0
2.67400	20	2	1	0
2.19400	20			
2.11400	10	2	2	0
1.99600	80	2	2	1
1.79800	100	3	1	1
1.72200	10	2	2	2
1.59700	20	3	2	1
1.49300	20	4	0	0

09-0205 — Wavelength= 1.54056

Cu3.8Ni

Copper Nickel

Rad: CuKa λ: 1.542 Filter: Ni Beta M d-sp: Debye-Scherrer

Cut off: Int: Estimation: I/Icor:

Ref: Long, Frazer, Ott, J. Am. Chem. Soc., 56, 1101 (1934)

Sys: Cubic S.G: F

a: 3.595 b: c: A: C:

α: β: γ: Z: mp:

Ref: Ibid

Dx: Dm: SS/FOM: F_7=12(.087, 7)

d Å	Int	h	k	l
2.08000	100	1	1	1
1.79700	80	2	0	0
1.26900	80	2	2	0
1.08400	100	3	1	1
1.03700	50	2	2	2
.898000	30	4	0	0
.825000	80	3	3	1

03-0879 — Wavelength= 1.54056

6CuO·Cu2O

Copper Oxide

Paramelaconite

Rad: CuKa1 λ: 1.5405 Filter: d-sp: Debye-Scherrer

Cut off: Int.: Estimation: I/Icor:

Ref: Frondel, C., Am. Mineral., 26, 664 (1941)

Sys: Tetragonal S.G: $I4_1/amd$ (141)

a: 5.83 b: c: 9.88 A: C: 1.6947

α: β: γ: Z: 2 mp:

Ref: Ibid.

Dx: 6.135 Dm: 6.106 SS/FOM: F_{20}=1(.162, 92)

d Å	Int	h	k	l
3.13000	20	1	1	2
2.90000	40	2	0	0
2.50000	100	2	0	2
2.47000	40	0	0	4
2.05000	60	2	1	3
1.88000	20	2	0	4
1.58000	80	2	2	4
1.45000	60	3	2	3
1.43000	60	2	0	6
1.25000	80	3	2	5
1.24000	40	2	1	7
1.06000	40	2	2	8
1.03000	20	4	4	0
1.02000	40	4	2	6
.951000	40	4	4	4
.941000	40	4	0	8
.937000	40	2	0	10
.918000	20	6	1	3
.861000	40	6	1	5
.834000	40			
.823000	20	0	0	12

References

[1] C. M. Perrott, Mining Applications of Thermal Sprayed Coatings, The Int. Jl. of Pow. Met. & Pow. Tech. 18(1) (1982) 39-55.

[2] B. C. Inwood, H. Meyer-Grunow, and P. E. Chandler, Optimisation of Plasma Sprayed Coatings and Powders for the Automotive Industry, The 12th Int. Conf. on Thermal Spraying 1 (1989) 101-111.

[3] W. Elger, A. Grubowski, J. Herbstritt, and S. Travis, Thermal Sprayed Plasma Wire Applications for the United States Navy, The 12th Int. Conf. on Thermal Spraying 1 (1989) 133-144.

[4] K. A. Gross, G. N. Haddad, and C. C. Berndt, Thermally Sprayed Coatings for Orthopaedic Applications, The 12th Int. Conf. on Thermal Spraying 1 (1989) 153-162.

[5] J. Ellis, Use of Chromium Carbide in Thermal Spray and Other Coating Technologies Pow. Met. 41(1) (1998) 18-19.

[6] D. G. McCartney, High Velocity Oxyfuel Thermal Sprayed Coatings : Processing, Characterisation, and Performance, Pow. Met. 41(1) (1998) 14-15.

[7] Y. Wang, Y. Jin, and S.Wen, The Friction and Wear Performance of Plasma-Sprayed Ceramic Coatings at High Temperature, Wear 129 (1989) 223-234.

[8] R. C. Tucker. Jr, Structure Property Relationship in Deposits Produced by Plasma Spray and Detonation Gun Techniques, J. Vac. Sci. Technol 11(4) (1974) 725-734.

[9] Advanced Surface Coatings, Edited by D. S. Rickerby and A. Matthews, Blackie & Sons Limited, Glasgow (1991) 217-243.

[10] Materials Degradation and its Control by Surface Engineering, Edited by A. W. Batchelor, L. N. Lam, and M. Chandrasekaran, World Scientific Publishing Co. Pte. Ltd., Imperial College Press (1999) 226-231.

[11] T. N. Rhys-Jones, Applications of Thermally Sprayed Coating Systems in Aero Engines, The 12th International Conference on Thermal Spraying 1 (1989) 87-99.

[12] Erich. Lugscheider, Christian Herbst, Lidong Zhao, Parameter Studies on High Velocity Oxy-Fuel Spraying, Surf. and Coating. Technol. 108-109 (1998) 16-23.

[13] G. Bechtloff and R. Potzl, Tests on the Influence of Processing Parameters Regarding the Structure and Hardness of Sprayed Hard-Metal Coatings on Light-Metal Substrates, The 12th International Conference on Thermal Spraying 2 (1989) 323-332.

[14] Shigeru Kitahara and Atsushi Hasui, A Study on the Bonding Mechanism of Sprayed Coatings, J Vac. Sc. Technol 11(4) (1974) 747-753.

[15] Brian S. Schorr, Kevin J.Stein and Arnold R. Marder, Characterisation of Thermal Spray Coatings, Mat. Charac. 42 (1999) 93-100.

[16] C. W. Smith, Science and Technology of Surface Coating, Edited by Brian. N. Chapman and J. C. Anderson, London, Academic Press (1974) 262-269.

[17] Design and Analysis of Experiments, Third Edition, Douglas C. Montgomery, John Wiley & Sons (1991) 546-548.

[18] Metallography, Structures, and Phase Diagrams, Metals Handbook 8 , American Society for Metals, 8th Edition (1978) 137.

[19] Quantitative Microscopy, Edited by Robert T. Dehoff, Frederick N. Rhines, McGraw-Hill Book Company (1968) 29-32.

[20] B. D. Cullity, Elements of X-ray Diffraction, Second Edition, Addison-Wesley Publishing Company, Inc., Menlo Park (1978) 411-415.

[21] D. L. Houck, New Powder Developments for Non-Transferred Plasma Arc Spraying, The Int. Jl. of Pow. Met. & Pow. Tech. 18(1) (1982) 69-79.

[22] Private Communication with Personnel at 4BRD, Chakeri.

[23] K. Ghosh, T. Troczynski, and A. C. Chaklader, Processing of Composite Al/SiC Powders for Plasma Spraying, The Int. Jl. of Pow. Met. 35(2) (1999) 27-35.

A 130849

Date Slip

This book is to be returned on the date last stamped.